

HERA-*g*, A NEW EXPERIMENT FOR GLUEBALL, HYBRID AND ODDERON STUDIES AT DESY

Proposal for a new experimental program using the
existing HERA-*B* detector.

T. Lohse, M. zur Nedden
Humboldt University, Berlin, Germany

M. Bargiotti, A. Bertin, M. Bruschi, M. Capponi, A. Carbone, S. De Castro, L. Fabbri,
P. Faccioli, D. Galli, B. Giacobbe, U. Marconi, I. Massa, M. Piccinini, M. Poli,
N. Semprini-Cesari, R. Spighi, S. Vecchi, M. Villa, A. Vitale, A. Zoccoli
*Dipartimento di Fisica, Università di Bologna and INFN Sezione di Bologna, Bologna,
Italy*

A. Bianconi, M. Corradini, A. Donzella, E. Lodi Rizzini, L. Venturelli, N. Zurlo
*Dipartimento di Chimica e Fisica per l'Ingegneria e per i Materiali, Università di Brescia
and INFN Gruppo Associato Brescia, Brescia, Italy*

Yu. Kiryushin, A. Lanyov, D. Pose, S. Resnikov, S. Somov, G. Evgrafov, I. Belotelov
Joint Institute for Nuclear Research, Dubna, Russia

M.A. Reyes, J. Felix
Universidad de Guanajuato, Mexico

M. Medinnis
DESY, Hamburg, Germany

M. Brauer^a, J. Spengler
Max-Planck-Institut für Kernphysik, Heidelberg, Germany
^a on leave of absence

V. Pugatch, Yu. Vassiliev, V. Aushev, S. Prystupa, Yu. Pavlenko, V. Kyva,
M. Molodyko
Institute for Nuclear Research, Ukrainian Academy of Science, Kiev, Ukraine

J.D. Hansen, R. Muresan
Niels Bohr Institutet, DK 2100 København, Danmark

M. Staric, R. Pestotnik, A. Stanovnik
Institut J. Stefan and Oddelek za fiziko, Univerza v Ljubljani, Ljubljana, Slovenia

S. Erhan, P. Schlein
University of California, Los Angeles, CA 90024, USA

G. Medin
Faculty of Science, Department of Physics, Montenegro University, Montenegro

A. Bogatyrev, V. Balagura, M. Danilov, F. Khasanov, B. Fominykh, R. Mizuk,
I. Matchikilian, I. Rostovtseva, V. Popov, S. Esenov, S. Shuvalov, I. Tikhomirov
Yu. Zaitsev

Institute of Theoretical and Experimental Physics, Moscow, Russia

S. Aplin^b, V. Galkin, A. Golovin, D. Rizhikov, V. Saveliev, M. Zaboudko
Obninsk State University, Obninsk, Russia

^b *University of Portsmouth, Portsmouth, Hampshire U.K.*

Y. Arestov, B. Chuiko, D. Konstantinov, V. Lishin, V. Shelikhov
IHEP, Protvino, Russia

L. Ferrero, R. Garfagnini, G. Piragino
*Dipartimento di Fisica Generale dell' Università di Torino and INFN Sezione di Torino,
Torino, Italy*

Corresponding Authors : Marco Bruschi (bruschi@bo.infn.it), Peter Schlein (schlein@ucla.edu)

Abstract

We propose a new, but relatively short, experimental program at HERA to use the existing HERA-*B* detector to run in the 920 GeV proton beam to study the production and decay properties of centrally-produced glueballs and hybrid mesons (the latter produced in Pomeron-Reggeon collisions). A search for Odderon-Exchange will also be carried out by measuring isolated centrally-produced $I=0$, $C=-1$ states such as ω^0 . A Level-1 trigger based on rapidity-gap vetoes at small and large angles outside the spectrometer aperture will efficiently select these events. We show the properties of such events extracted offline from $> 7 \cdot 10^7$ triggered events, corresponding to about 5 minutes of data taking with such a rapidity-gap trigger. For example, a 100 hour data-taking run in the manner described herein will already yield a factor of 1000 times more data than displayed in this Proposal. Such a data sample would allow fundamental contributions to be made to a number of important fields. These data would correspond, for example, to a factor of ~ 40 increase in the number of $\pi^0\pi^0$ events with mass, $M > 2$ GeV, published by the WA-102 collaboration.

Physicists and Institutes interested in participating in this project are asked to contact at the earliest possible time the corresponding authors.

Contents

1	Introduction	6
2	Status of glueball and hybrid physics	6
3	HERA-<i>B</i> detector	7
3.1	Inner tracker	9
3.2	Rapidity-Gap Triggering	9
3.3	Level-1 Trigger scheme for HERA- <i>g</i>	12
4	Double-<i>Pomeron</i>-Exchange in Experiment UA8 and predictions for HERA-<i>g</i>	13
4.1	HERA- <i>g</i> kinematics	14
5	Monte-Carlo acceptance calculations for HERA-<i>g</i>	17
6	Extracting DPE events from 2002-2003 minimum-bias data	21
6.1	Selection program	22
6.2	Central $\pi^+\pi^-$ and $\pi^0\pi^0$ systems	24
6.3	Nuclear effects	26
7	Monte Carlo simulations of inelastic events	29
7.1	Inelastic background suppression by means of rapidity gap vetoing system .	29
7.2	HERA- <i>g</i> rates for centrally produced final states	30
8	P_t^2 distributions and ϕ correlations	36
9	Other channels, DPE or <i>Reggeon</i>-Exchange	37
9.1	$K_s^0 K_s^0$ and $K^+ K^-$	37
9.2	$\eta\pi^+\pi^-$ in $2\gamma\pi^+\pi^-$ final state	39
9.3	η and ω^0 in $2\gamma\pi^+\pi^-$ final state	41
9.4	$\pi^+\pi^-\pi^+\pi^-$ in 4-track events	42
9.5	$K_s^0 K^\pm\pi^\mp$ in 4-track events	43
9.6	Hybrid search in <i>Pomeron-Reggeon</i> collisions using $\eta\pi^\pm$ in $\gamma\gamma\pi^\pm$ events	45
9.7	ρ^\pm and <i>Reggeon</i> -Exchange	46
9.8	$\gamma\gamma$ final state	47
9.9	Statistics achievable by HERA- <i>g</i>	48
10	Proposed Program	50
10.1	Manpower needs	50
11	Conclusions	51

LIST OF THE ABBREVIATIONS COMMONLY USED IN THE TEXT

2002/2003: HERA-*B* data taking for the years 2002 and 2003
DAQ: Data Acquisition
DPE: Double Pomeron Exchange
ECAL: Electromagnetic CALorimeter detector
GEM: Grid Electron Multiplier
ITR: Inner Tracker Detector
LAC: Large Angle Scintillator counters
LEGO: Three dimensional displaying of plots *a' la lego*
MC: Monte Carlo
MSGC: Micro Strip Gas Chamber
MUON: Muon detector
OTR: Outer Tracker Detector
RICH: Ring Imaging Cherenkov Counter
SAC: Small Angle Scintillator counters
SiPM: Silicon PhotoMultiplier
VDS: Silicon Vertex Detector

1 Introduction

We propose a new experiment, HERA- g , to study glueball and hybrid states at DESY using the existing HERA- B spectrometer. These will be produced in another class of centrally-produced systems than are B-mesons, namely those that are formed in the interactions of color-singlet components on the beam baryons. Such interactions are characterized by the absence in the observed event of any particles other than those which are part of the centrally-produced system. There are 1.5 to 2.0 units of rapidity outside the spectrometer aperture, both at small and large angles, which are devoid of particles. We refer to such events as “rapidity-gap events”.

Since significant numbers of HERA- B collaborators have left the collaboration, it was decided that any further physics program using the HERA- B spectrometer should be proposed by a new collaboration comprising a core of remaining HERA- B groups, together with as many new collaborators as possible. We anticipate that additional groups will join during the evaluation period of this proposal by the DESY PRC and Management. Some of the collaborators of the present proposal have a high level of experience with the main physics themes discussed herein.

We plan to study the following three classes of events:

1. Double- \mathcal{P} omeronExchange (“DPE”): As discussed below, the interactions of the dominantly digluon clusters which we call \mathcal{P} omerons constitute a favored mechanism to produce the bound gluon systems called “glueballs”.
2. \mathcal{P} omeron- \mathcal{R} eggeon-Exchange: This type of exchange may be optimal for producing the bound quark-antiquark-gluon states called “hybrids”.
3. \mathcal{P} omeron- \mathcal{O} dderon-Exchange: Search for central production of isolated $I=0$, $C=-1$ states which may provide evidence for this production mechanism. The “ \mathcal{O} dderon” is a putative 3-gluon state in the proton sea with negative C-parity.

The main strength of HERA- g , aside from the quality of its spectrometer and the advantages of its 920 GeV beam energy, is that its flexible high-speed pipelined triggering and data acquisition system will allow us to obtain an orders-of-magnitude statistics improvement over previous experiments. This should allow major advances in the understanding of glueball and hybrid spectra.

In the body of this proposal, we show real DPE data extracted from more than $7 \cdot 10^7$ triggered HERA- B events. These data would correspond to about 5 minutes of running HERA- g with the proposed rapidity-gap Level-1 trigger. Thus, in 100-hours of data-taking, which we propose here, we should acquire more than 1000 times the data shown in the following pages.

For example, the $\sim 2000 \pi^0\pi^0$ events on hand would multiply to more than 2 million such events (see Section 7.2). This is 10 times more events than published by the WA-102 Collaboration [1], who studied centrally final systems in pp interactions at 450 GeV. Additionally, our higher beam energy compared to WA-102 means that we have an additional factor of 3.5 (see Section 4.1) more events with central mass, $M_X > 2$ GeV. Thus, in this higher mass region, we will have an effective factor of about 40 times more events than WA-102. Thus, HERA- g is perfectly suited to be the “next-generation WA-102 experiment”

2 Status of glueball and hybrid physics

The fundamental properties of QCD imply the existence of additional families of

mesons made of bound gluons (“glueballs”) or quark-antiquark states with a gluon (“hybrids”). Lattice QCD predicts both the glueball [2] and hybrid [3] spectra. The basic features of these expected spectra have been summarized for the Review of Particle Physics by Amsler [4]. The lightest glueballs have quantum numbers $J^{PC} = 0^{++}$ and 2^{++} , with expected masses of about 1600 and 2230 MeV, respectively. Candidates for both of these have been reported. The 0^{-+} state and others with quantum numbers forbidden for quark-antiquark systems are expected to have masses above 2 GeV. The ground-state hybrids, 0^{-+} , 1^{-+} , 1^{--} and 2^{-+} , are expected to occur in the 1.7 to 1.9 GeV region. Candidates for these states have also been reported [4].

3 HERA-*B* detector

A sketch of the HERA-*B* detector is shown in Fig. 1. Full descriptions of its detector subsystems are accessible at the HERA-*B* website address: <http://www-hera-b.desy.de/general/publications/description/welcome.html>

The conical vacuum pipe at far right contains the target-wire system and seven of the eight silicon-vertex-detector (VDS) measuring stations. We discuss some aspects of the VDS system in the following subsection on triggering. The bulk of the data shown in this proposal was taken with a Carbon wire target, while there is some data taken with Tungsten and Titanium wire targets.

The detector was designed to optimally measure systems produced at Feynman- $x_F = 0$ in the reaction center-of-mass. With a proton beam energy of 920 GeV on a fixed target, a system with mass M travels forward in the laboratory with energy, $E = \gamma M = 21M$. Thus, a system with 2 GeV mass has an energy of 42 GeV in the laboratory.

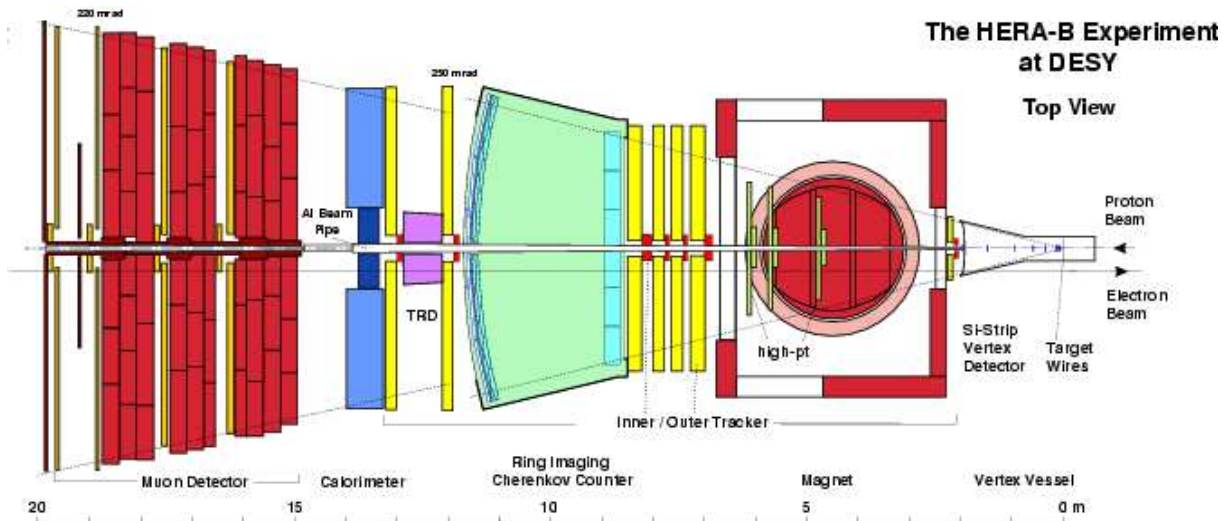


Figure 1: *Sketch of the HERA-*B* detector. The incident 920 GeV proton beam travels from right to left. Target wires and silicon vertex detector are in the conical vacuum tank at the right-hand side of the sketch.*

We summarize the recent history of the detector: With the exceptions of the inner tracker and di-lepton Level-1 trigger, HERA-*B* was largely completed by early 2000. The detector was brought into operation by the middle of 2000. The long HERA shutdown ending in 2001 afforded the opportunity to complete the HERA-*B* detector and trigger system and also to remedy the problems found during the year-2000 running period. After the shutdown and while the HERA team concentrated mainly on commissioning

high luminosity collider operation and understanding the debilitating backgrounds seen by the collider experiments, they were nonetheless able to fit periods of stable proton running into their busy schedule. These periods were used to tune the newly completed HERA-*B* system. The efforts in the shutdown were largely successful. The following improvements are relevant for HERA-*g* :

- vastly improved performance of the electromagnetic calorimeter due mainly to improved coupling of signals from the detector to the readout electronics;
- a more-than-tenfold decrease in the rate of high voltage failures in the outer tracker (obtained by a complete disassembly of the system to replace incorrectly mounted capacitors) resulting in more efficient tracking, both at the trigger level and in the offline reconstruction;
- improved stability and a tenfold increase in throughput of the data acquisition system. Final commissioning of the control software was completed. The control system is built around the data acquisition system and provides for event distribution, routing of geometry and calibration constants and monitoring;
- an upgrade of the 240-node Level-2 trigger farm from 400 MHz to 1.3 GHz processors. We are now able to transform our two trigger farms (Level-2 and Level-3)¹ into dedicated reconstruction or Monte Carlo generation machines in the periods between luminosity fills. The event reconstruction rate with both farms working is nearly equal to the trigger rate, implying that fully reconstructed events become available for analysis within hours or days of having been collected.

In addition, the following other improvements were made, which are not of direct interest to HERA-*g* , since the complex first-level tracking machinery is not needed to achieve the main goals of HERA-*g* . However, if the need should later arise, we could have efficient triggering on leptonic final states.

- The introduction into the trigger of track-following in both the muon system and the outer tracker in the Level-1 trigger;
- a better performance of the muon system, due both to increased immunity to noise – the result of preamplifier modifications, and to extensive work to repair broken channels and improve system stability;
- a completely new and improved muon detector tracking algorithm in the Level-2 trigger.

The good system performance during the 2002/3 data-taking period has allowed an investigation into its capabilities for studying the production and decay of glueballs and hybrids in central interactions. While analysis of the resulting test data samples is ongoing, we show some preliminary results in this proposal. The results of this study allow us to conclude that the existing detector is ideal for a next-generation experiment, HERA-*g*, on this physics.

¹“Level-3” was called “Level-4” by the HERA-*B* Collaboration.

3.1 Inner tracker

Some special comment is due for the Inner Tracker system (ITR) of the HERA-*B* experiment. In the 2002/2003 configuration it consisted of a MSGC GEM chamber placed just before the magnet (MS01), four such chambers placed just after the magnet (PC1 to PC4), and two chambers (TC1 and TC2) placed between RICH and ECAL.

The ITR system showed problems in nearly all chambers of the stations which, in the original plans for the 2002/2003 data taking, should have contributed to the Level-1 (PC1 and PC4, TC1 and TC2): the chambers themselves operate correctly, but large groups of readout strips are shorted to each other, thus effectively giving large regions of zero efficiency ².

Still, the chambers MS01 (in front of the magnet) and PC2 and PC3 were not modified during the shutdown in 2001 and can be operated at single-hit efficiencies of about 90 ÷ 95%.

The typical event of HERA-*g* will be characterized by low track multiplicity in the detector (the level of uncorrelated hits will be low) and the considerable redundancy foreseen for the HERA-*B* tracking will be unnecessary. Moreover **HERA-*g* will not use the tracking system at the Level-1**. Therefore we propose the following strategy for the ITR:

- MS01 and PC2 and PC3 were not suited to give signals to the HERA-*B* First Level Trigger (the chip version used in these stations has serious feedback problems which prevent the use of the on-chip comparators). They could, however, be used on the HERA-*g* Level-2 and in the off-line reconstruction. We therefore could move PC2 and PC3 to the place of PC1 and PC4 to get a better lever arm for track reconstruction.
- We will combine good, working chambers of PC1 and PC4 into a newly-built station to be placed in the position of PC3 (this position being optimal for multiple scattering and track resolution motivations).
- In case it will be worthwhile and feasible, we will combine good, working chambers of TC1 and TC2 into a newly-built station to be placed in the position of TC2.
- We will remove the unused stations from the beam-line, since they will just provide unwanted material.

The performance of the track reconstruction with the proposed configuration has yet to be studied in detail. Nevertheless the present status of the available detector appears sufficient for HERA-*g* purposes.

Switching on the ITR after a half a year of so of no beam operation could be problematic. Although the detectors are being flushed with clean, dry nitrogen, we can not exclude that they would require another on-beam training period. Most probably this wouldn't need to be as long as in 2002 (two months of training were necessary).

We are confident to set up a satisfactory ITR for HERA-*g* with the existing detector, the only critical point being manpower (as explained in Sec. 10.1).

The non-availability of the ITR would cost, as we can extrapolate from the present analysis, a factor 2 in statistics in the $\pi^+\pi^-$ and a factor 3 in the $\pi^+\pi^-\pi^+\pi^-$ final states.

3.2 Rapidity-Gap Triggering

Rapidity-gap veto counters will be a main component of the Level-1 trigger. They

²The culprit is the z-bonding connection between the readout electronics and the chambers.

will be combined with a version of minimum-bias interaction requirements based on the electromagnetic calorimeter (ECAL).

The spectrometer has a target monitoring and control system which maintains a fixed desired interaction rate. We plan to run initially with a Carbon target wire ³ to yield a 1 *MHz* interaction rate. The target station 1 (closer to the detector) will be the used one, to maximize the acceptance at large angle. With the HERA bunch rate of 10 *MHz*, the average number of interactions per bunch crossing will therefore be 0.1. With uniform bunch population, 6.3% of the events will have more than one interaction in them. However, since more than 99% of the interactions do not have rapidity gaps, these bunches will be removed in the Level-1 trigger by the rapidity-gap veto counters.

There are two additional levels of triggering in the HERA-*B* data-acquisition system. Both of these use processor farms. Level-2 contains 240 nodes of 1.3 GHz processors, while Level-3 contains 100 nodes of dual 0.5 GHz processors. In order to maintain an approximately dead-time-free DAQ environment, the limiting rate into Level-2 should be 10 kHz, while that into Level-3 should be 1 kHz.

With the maximum allowed input rate of 10 kHz to the Level-2 processor farm, the Level-1 trigger must achieve a factor of 100 suppression of inelastic interactions. We will show (see Sec. 7.1) that a factor of *at least* 100 suppression can be obtained in the Level-1 trigger with the use of rapidity-gap counters both at small and large angles in the laboratory.

The ITEP group prior to the 2002/2003 running period, installed a system of four Small-Angle Scintillation Counters (SAC) which cover the laboratory angular region, $2.3 < \theta < 9.6$ mrad, outside the proton beam pipe in front of the muon system. This corresponds to a rapidity-gap in the center-of-mass of 1.5 units. We find that these counters in veto yield a factor of 10 suppression of inelastic events from the interaction trigger (as defined in Sect. 6), with a further efficiency of more than 90% in rejecting empty bunches. In order to understand this factor of 10 suppression, we used our Monte-Carlo inelastic event generator and found that 1/9 of all such events have one or more charged tracks or γ s in this angular region, in good agreement with our observations (see Section 7.1).

For the large-angle rapidity-gap veto, corresponding to the backward direction in the center-of-mass, we have shown with inelastic interaction Monte Carlo events that we can obtain at least the required additional factor of 10 suppression by vetoing in the angular region $\sim 0.2 < \theta < \sim 1.0$ rad (see Sect. 7.1). This can be achieved by replacing the first silicon station in the VDS by scintillation counters and using them in the Level-1 trigger. Scintillator sizes up to the needed dimensions can be accommodated by the present pot without major modifications. It is also relevant to note that, although the maximum vertical acceptance angle of the spectrometer is 160 mrad and the horizontal (bending plane) acceptance angle is about 250 mrad, the maximum effective angular acceptances for the dipion events discussed below are about 120 and 180 mrad, respectively. Thus, we can easily have rapidity gaps of at least 1.5 units, both at small and large angles. This should be adequate at our c.m. energy.

Figure 2 shows a perspective view of the eight silicon measuring stations installed inside the vacuum tank and a side view of one quadrant of the detectors. The 10 mrad

³We briefly recall here that the HERA-*B* experiment can take data using different target materials. There are 8 wires subdivided into two target stations: one closer to the detector (identified by the index 1) and one positioned about 4 cm further (identified by the index 2). The four wires of each station are identified by the letters a (above), b (below), i (inner), o (outer). Therefore in the following C-b1, for example, will identify the Carbon wire “below” belonging to the wire station 1 (closer to the detector) positioned in the beam halo.

The possibility to take data with different materials could play an important role for HERA-*g* (see Section 6.3).

minimum acceptance angle is seen. We also see that the first measuring station is not a critical element of the silicon tracking system and therefore that it can be replaced by scintillation counters for use in the Level-1 trigger.

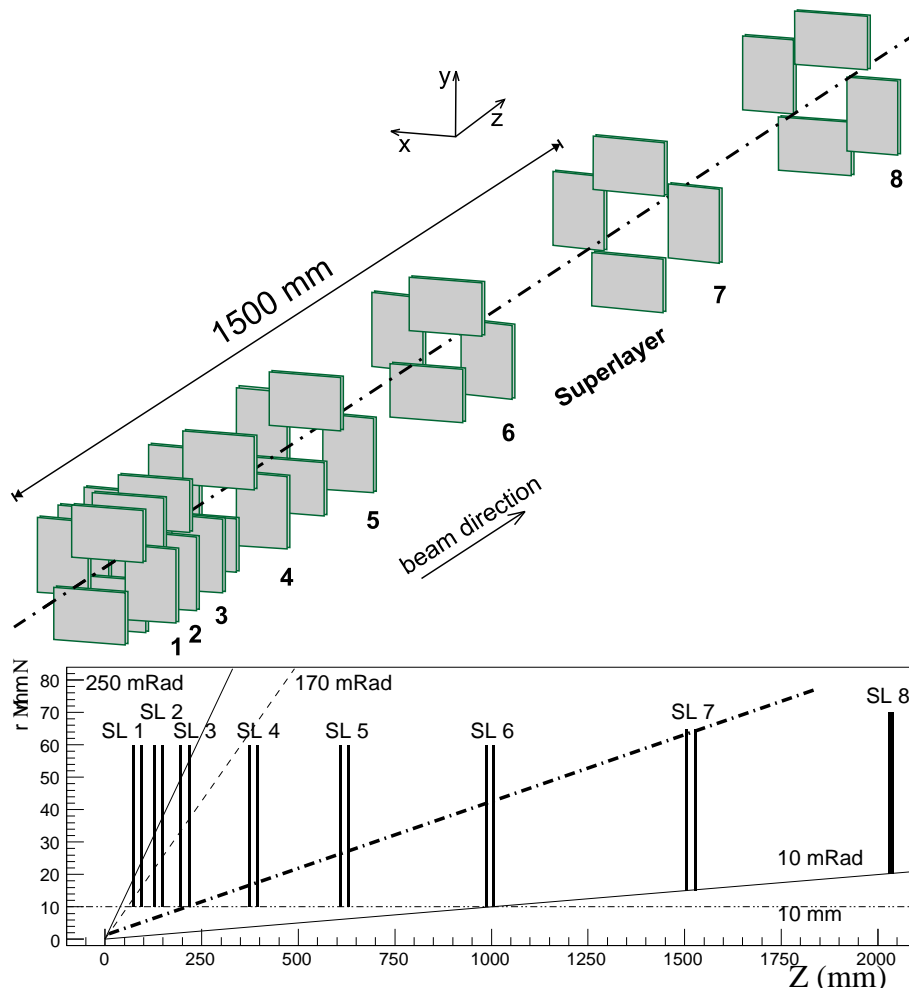


Figure 2: *Upper: Perspective drawing of the VDS stations inside the vacuum tank; Lower: Side view of one quadrant of silicon detectors with the angles of minimal and maximal acceptance (for both the projections perpendicular to the beam) shown. The dashed-dotted line is a typical intermediate track direction showing intercepts with various silicon measuring stations.*

The backward veto scintillator counters (LAC) can be fixed on a support structure of the first VDS layer. Their thickness will be 5 mm and they will cover the pseudo-rapidity range from $\eta \simeq 2.3$ to $\eta \simeq 0.6$ ⁴. Light will be collected using wave length shifter (WLS) fibers embedded into the grooves in the scintillator. The light will be detected by a novel photodetector, so called Si Photo Multiplier (SiPM). This tiny (few mm^3) detector can be also embedded into the scintillator. SiPM does not require HV (only about 60V bias voltage) and a light guide. Therefore existing feedthroughs can be used for power and signal connections.

More than 100 of such counters with the size of $50 \times 50 \times 5 \text{ mm}^3$ have been made and tested at ITEP for a Linear Collider calorimeter prototype. Fig. 3 shows the counter response to a Sr90 source (amplitude less than 400 adc counts) and LED test pulses where individual photoelectron signals are clearly seen.

⁴Some converter material will be put in front of the LAC to force gammas conversion.

Thus, we expect to be able to achieve at least a factor of 1/100 minimum-bias suppression with the full system of rapidity-gap veto counters. This matches well to the 10 kHz input-rate capability of our Level-2 processor farm: 1/100 of the 1 MHz interaction rate yields 10 kHz inelastic interaction rate.

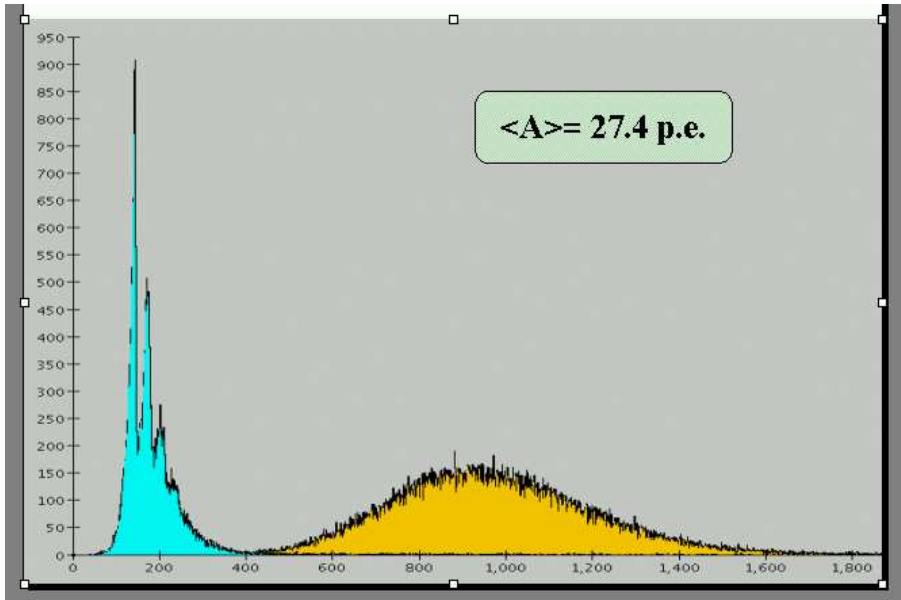


Figure 3: *Scintillator counter response to a Sr90 source (adc count less than 400) and LED test pulses. The individual photoelectron signals are clearly seen.*

3.3 Level-1 Trigger scheme for HERA-*g*

In the Level-1 trigger scheme we propose for HERA-*g* we will use a simplified and robust version of the Level-1 designed for HERA-*B*. First of all we must stress that **HERA-*g* will not perform any tracking at the Level-1**. The interaction triggering will be provided by the ECAL pretrigger system [5] whose output will be fed into existing Multiplexer Cards and then into the Track Decision Unit (TDU) [6] used in counting mode. This configuration has been already successfully used in the 2002/2003 ECAL interaction trigger data taking as explained in Sect. 6. An interaction will be identified by requiring at least one cluster having transverse energy E_T greater than a preset threshold (0.15 GeV in 2002/2003).

The rapidity gap vetoing will be obtained by feeding the SAC and LAC signals, in logical “OR” and properly delayed, into the ECAL pretrigger system, after a fan-out distribution of them. The ECAL pretrigger scheme contains, in fact, the capability to be inhibited by an external signal fed into the Fast Control System (FCS) cards [6] distributing the HERA clock to the experiment.

The two surviving elements of the original HERA-*B* Level-1 scheme, the ECAL pretrigger (with five spare boards out of 128 cards installed) and the TDU (with one spare board), have ran in a stable and reliable way during the last years of HERA-*B*.

4 Double- \mathcal{P} omeron-Exchange in Experiment UA8 and predictions for HERA- g

In the so-called Double- \mathcal{P} omeron-Exchange (DPE) process:

$$pp \rightarrow p X p \quad (1)$$

and its analogue $p\bar{p}$ process, the central X systems are produced by collisions of “sea” partons in the beam and target particles. The baryons continue on their way, relatively unperturbed. The UA8 [7] and H1 [8] experiments have shown us that there are digluon clusters in the parton sea⁵, which possess a most likely momentum fraction of their host baryon near zero. These empirical colorless objects are what we call “ \mathcal{P} omerons”. The absence of particles between X and the two outgoing beam particles are “rapidity gaps”, the presence of which is a signature for the exchange of colorless objects from both beam baryons.

These \mathcal{P} omeron systems, which carry a small fraction of the beam momentum of the two approaching hadrons, $\Delta p/p = \xi = 1 - x_p$, can collide and then constitute the entire effective interaction between the two beam particles. The system X with invariant mass, M_X , is the result of the \mathcal{P} omeron- \mathcal{P} omeron interaction. The DPE process is the closest we can come to pure gluon interactions and, as such, should be a splendid glueball production process [9].

It should be noted, however, that even with the presence of rapidity gaps, \mathcal{R} eggeon- and perhaps \mathcal{O} dderon-Exchanges can also occur. In the body of this proposal we point to the possible consequences of these exchanges.

Figure 4 shows the total \mathcal{P} omeron- \mathcal{P} omeron cross section measured by the UA8 collaboration [10] using React. 1. In that experiment, there were two classes of events. In the “AND” events, both final-state proton and antiproton were observed and had the same azimuthal angle. Thus, the difference in transverse momentum of the two protons, whose distribution was shown by the WA-102 experiment to correlate with the spin-parity of the produced central system [11, 12, 13], is on the average, $\Delta P_T = 0$. The other proton configuration, called “OR”, typically has $\Delta P_T = 1$. GeV. We see that the AND data, whose proton configuration WA-102 says correlates with its glueball candidates, have a larger cross section which rises from 1.5 to 3.5 mb within a mass range of a few GeV. UA8 suggests that the rise seen in the figure is likely a manifestation of glueball production. Above a mass of about 10 GeV, the agreement with the solid curve tests the validity of factorization.

The differential cross section for the DPE process⁶ is:

$$\frac{d^6\sigma_{DPE}}{d\xi_1 d\xi_2 dt_1 dt_2 d\phi_1 d\phi_2} = F_{\mathcal{P}/p}(t_1, \xi_1) \cdot F_{\mathcal{P}/p}(t_2, \xi_2) \cdot \sigma_{\mathcal{P}\mathcal{P}}^{tot}(s') \quad (2)$$

where the variables, (ξ_i, t_i, ϕ_i) , are the momentum fraction, momentum transfer and azimuthal angle of the outgoing protons (or emitted \mathcal{P} omerons) in React. 1, and s' is the squared mass, M_X^2 , of the central system in React. 1. The flux factors, $F_{\mathcal{P}/p}(t, \xi)$, in Eqn. 2 are dominated by the Regge factor which, at low- $|t|$, has the form: $1/\xi^{1+2\epsilon}$, where $1 + \epsilon = 1.08$ is the $t = 0$ intercept of the effective \mathcal{P} omeron Regge trajectory (at the HERA- g energy). Hence, at low $|t|$, the cross section is described by:

$$\sigma \approx \frac{1}{\xi_1^{1.16}} \cdot \frac{1}{\xi_2^{1.16}} \cdot \sigma_{\mathcal{P}\mathcal{P}}^{tot}(s'). \quad (3)$$

⁵The UA8 experiment discovered the partonic structure of these clusters and therefore, because their structure is “Super-Hard”, that they contain very few gluons (hence “digluon”). The H1 experiment showed that the structure of these clusters is more than 85% gluons.

⁶See Ref. [10] for the detailed form of the phenomenological flux factor.

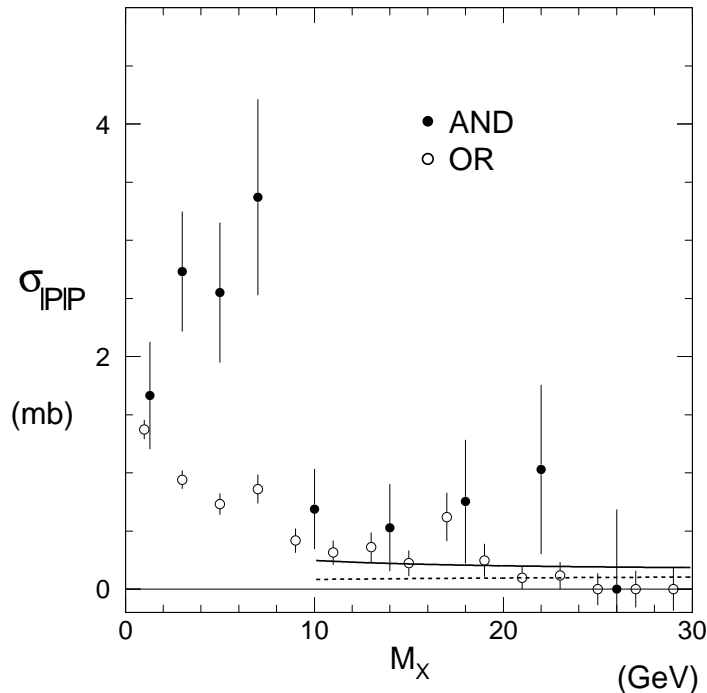


Figure 4: *Mass dependence of the Pomeron-Pomeron total cross section, shown separately for the “AND” ($\Delta P_T = 0$) and “OR” ($\Delta P_T = 1$ GeV) data samples.*

In the M_X region which is not dominated by large resonances (such as $f(1270)$), the ξ dependencies of Eqn. 3 should describe the data. That they do is shown below in Sect. 6.2.

Although there is no explicit ϕ -dependence on the right-hand-side of Eqn. 2 and the Pomerons are emitted independently and isotropically, some ϕ correlations result because significant regions in the 6-dimensional space, $(\xi_1, t_1, \phi_1, \xi_2, t_2, \phi_2)$, are unphysical and give $s' < 0$. More importantly, ϕ correlations have been observed [11, 12, 13] in React. 1 which are correlated with the spin-parity of the produced meson state in $\sigma_{\mathcal{P}\mathcal{P}}^{tot}$. We note here that ϕ correlations must kinematically be related with the observed transverse momentum of the central system in React. 1. Since in the present proposal, we do not intend to detect the final-state baryons, we calculate the expected P_T^2 distributions of the central system for each of the various ϕ distribution found by WA102. This is discussed below in Sects. 8 and 9.2.

4.1 HERA- g kinematics

Figure 5 shows the kinematics of the interacting color-singlet systems in the proton and quasi-free proton. They possess momentum fractions, ξ_1 and ξ_2 respectively, of their host baryons. The invariant mass of the centrally produced system and its Feynman- x_F in the proton-proton center-of-mass are given to good approximation by:

$$M_X^2 = \xi_1 \xi_2 s . \quad (4)$$

In the figure, curves of constant M_X are plotted in the $\xi_1 - \xi_2$ plane for the c.m. energy of HERA- g . Also shown are lines of constant $x_F = \xi_1 - \xi_2$ in the overall center-of-mass of React. 1:

$$x_F = \xi_1 - \xi_2 . \quad (5)$$

The significance of Fig. 5 is that, for each event, if we know M_X and x_F , then we also know its ξ_1 and ξ_2 . Conversely, if we have some understanding of the ξ dependencies of different possible exchanges, we can predict observed dependencies on M_X and x_F . We can see that, in the absence of dominant resonance-producing \mathcal{P} omeron- \mathcal{P} omeron interactions, the observed M_X distribution in a sample of data as well as its x_F distribution are determined by the ξ -distribution of a \mathcal{P} omeron in a proton. We show several examples of this predictive power in Sects. 6.2 and 6.3.

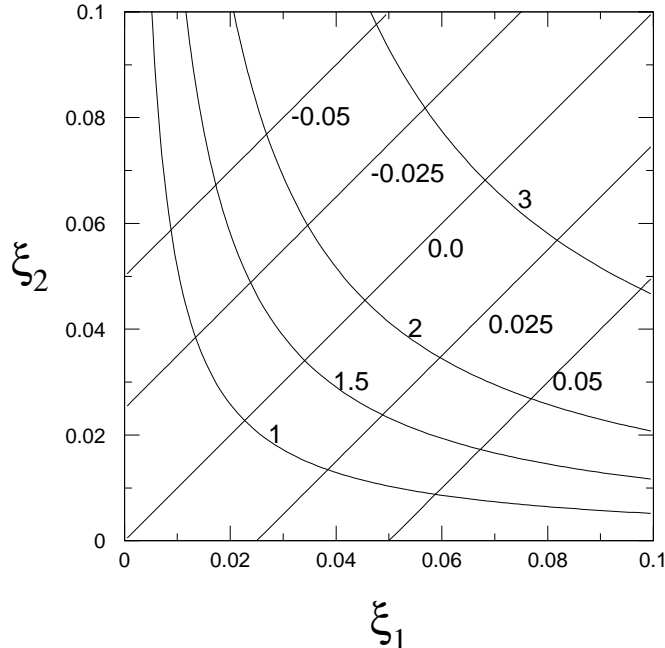


Figure 5: *Kinematics of HERA-g with 920 GeV proton beam. ξ_1 and ξ_2 are the momentum fractions of the beam proton and quasi-free nucleon in the Carbon possessed by the interacting color-singlet systems. Lines of constant Mass (GeV) and constant Feynman- x_F (in the c.m.) possessed by the centrally-produced system are shown.*

Figure 6 from Ref. [10] shows the predicted mass spectra for the DPE React. 1 at three different beam energies. 450 GeV was the beam energy of the WA-102 experiment. Since we shall see in Sect. 6.2 that 920 GeV prediction agrees with our observed $\pi^+\pi^-$ and $\pi^0\pi^0$ mass spectra in the mass region $M > 1.5$ GeV, we can have some confidence in the reliability of the predictions shown at 450 and 280 GeV. It is clear that HERA-g has much better capability in the higher mass regions. Table 1 shows the total DPE cross sections, assuming a total \mathcal{P} omeron- \mathcal{P} omeron cross section of 1.5 mb (see Fig. 4), as well as the integrals above several mass values.

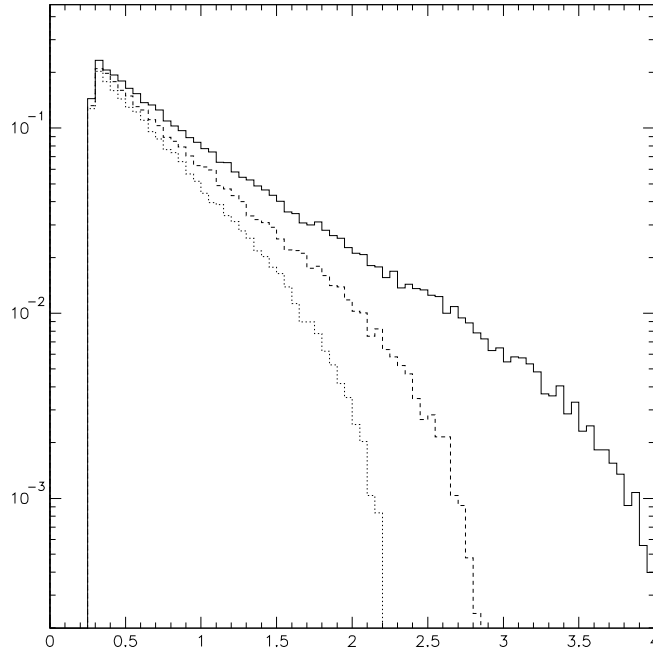


Figure 6: *UA8 Double-Pomeron-Exchange predictions of the differential cross section, $d\sigma/dM_X$ (mb/(0.05GeV)) vs. M_X (GeV) (integrated over all the t values). Reading from left to right, the three curves shown correspond to proton beam momenta of 280, 450 and 920 GeV, respectively. The horizontal scale is from 0 to 4 GeV central system mass. See Table 1 for the absolute cross section values assuming a Pomeron-Pomeron total cross section of 1.5 mb (see Fig. 4).*

	Beam Momenta		
Mass GeV	280 GeV	450 GeV	920 GeV
All	0.311 mb	0.384 mb	0.504 mb
> 1.5	4.5%	10.2%	18.5%
> 2.0	0.3%	2.7%	9.5%
> 2.5	–	0.4%	4.5%

Table 1: *Cross sections in mbarn for specific mass regions in Fig. 6 after normalizing the $d\sigma/dM_X$ curves to a total Pomeron-Pomeron cross section of 1.5 mb.*

5 Monte-Carlo acceptance calculations for HERA-g

In order to investigate the acceptance and reconstruction efficiencies of the HERA-B detector we have developed two types of Monte Carlo simulation.

A full Monte Carlo simulation in which the final state particles are passed through a GEANT-based detector simulation. These results are used to obtain our overall reconstruction efficiencies and tune our analysis codes and fast Monte-Carlo (see below). The resolutions and reconstruction efficiencies extracted from this simulation are summarized in Table 2 for a range of di-pion invariant masses and for the ECAL interaction trigger configuration (see Section 6).

Final State	$\pi^0\pi^0$	$\pi^0\pi^0$	$\pi^0\pi^0$	$\pi^+\pi^-$	$\pi^+\pi^-$	$\pi^+\pi^-$
$M(\text{GeV})$	1.0	1.5	2.0	1.0	1.5	2.0
$\sigma_{\gamma\gamma}(\text{MeV})$	8.8	7.7	7.6	-	-	-
$\sigma_M(\text{MeV})$	30	43	49	10	17	20
$\sigma_{x_F} \cdot 100$	0.07	0.09	0.10	0.02	0.03	0.04
$\sigma_{P_T}(\text{MeV})$	35	44	56	11	15	23
ϵ	0.07	0.09	0.11	0.14	0.14	0.14

Table 2: Resolutions of reconstructed quantities and overall reconstruction efficiency, ϵ , obtained with the full Monte Carlo simulation for the final states: $\pi^0\pi^0 \rightarrow 4\gamma$ and $\pi^+\pi^-$. The dipion systems have been generated at $x_F = 0$ and $P_T = 0$ for three different mass values ($M = 1, 1.5, 2.0$ GeV). $\sigma_{\gamma\gamma}$ is the resolution of the reconstructed π^0 mass. The efficiency refers to the ECAL interaction trigger configuration (see Section 6).

A fast Monte Carlo simulation has been used for preliminary studies of the geometric acceptance of the spectrometer. In particular, we demonstrate that the acceptance in the $\cos(\theta) - \phi$ “decay” angular distribution⁷ of central systems will allow us to reconstruct spherical harmonic moments with sufficiently high ℓ -values to carry out the necessary phase-shift analysis.

In the Figures 7 and 8, we show $\cos(\theta) - \phi$ LEGO plots of the geometric acceptance for the 4γ final states from $\pi^0\pi^0$ with a mass of 2 GeV and $\eta\eta$ with a mass of 2.5 GeV, respectively. In each case nine distributions are shown for all combinations of transverse momentum, $P_t = 0, 0.5$ and 1.0 GeV and $x_F = -0.05, 0.0$ and $+0.05$ of the system in the overall center-of-mass. We see that there are no significant holes in the $\cos(\theta) - \phi$ acceptance that would compromise the acceptance corrections.

Figures 9 show the geometrical acceptances for $\pi^+\pi^-$ and $\pi^0\pi^0$ events calculated with the fast Monte-Carlo as a function of invariant mass for three values of Feynman- x_F . These distributions illustrate two main points:

- The acceptance grows with increasing mass;
- The acceptances peak at $x_F = 0$.

⁷ θ is the angle between a π^0 direction and the $\pi^0\pi^0$ flight direction in the $\pi^0\pi^0$ center-of-mass and ϕ is its azimuthal angle measured with respect to the production plane of the dipion system.

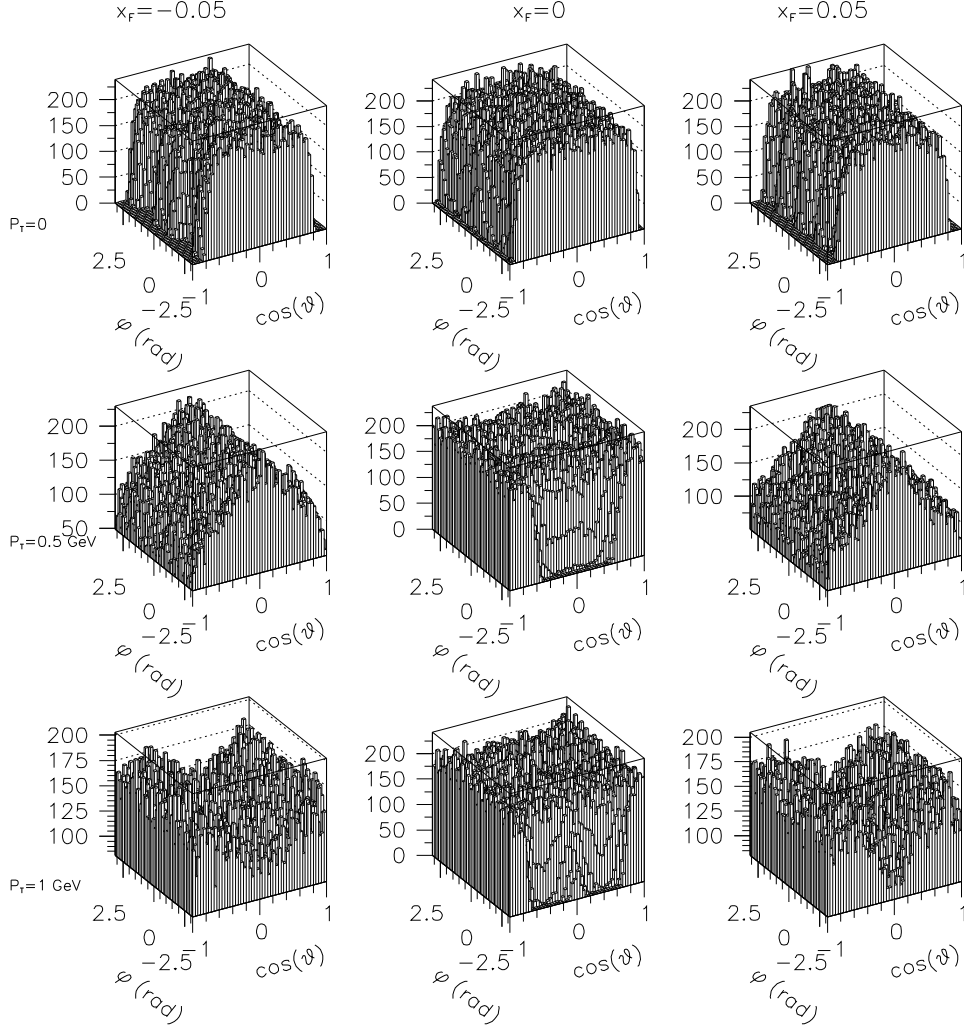


Figure 7: *LEGO* plots of the $\cos(\theta) - \phi$ geometric acceptance (not normalized) for a system with mass 2.0 GeV decaying in $\pi^0\pi^0 \rightarrow 4\gamma$. The nine plots shown are for the different combinations of $x_F = -0.05, 0.0, +0.05$ and $P_t = 0.0, 0.5, 1.0 \text{ GeV}$ values of the dipion system in the overall center-of-mass.

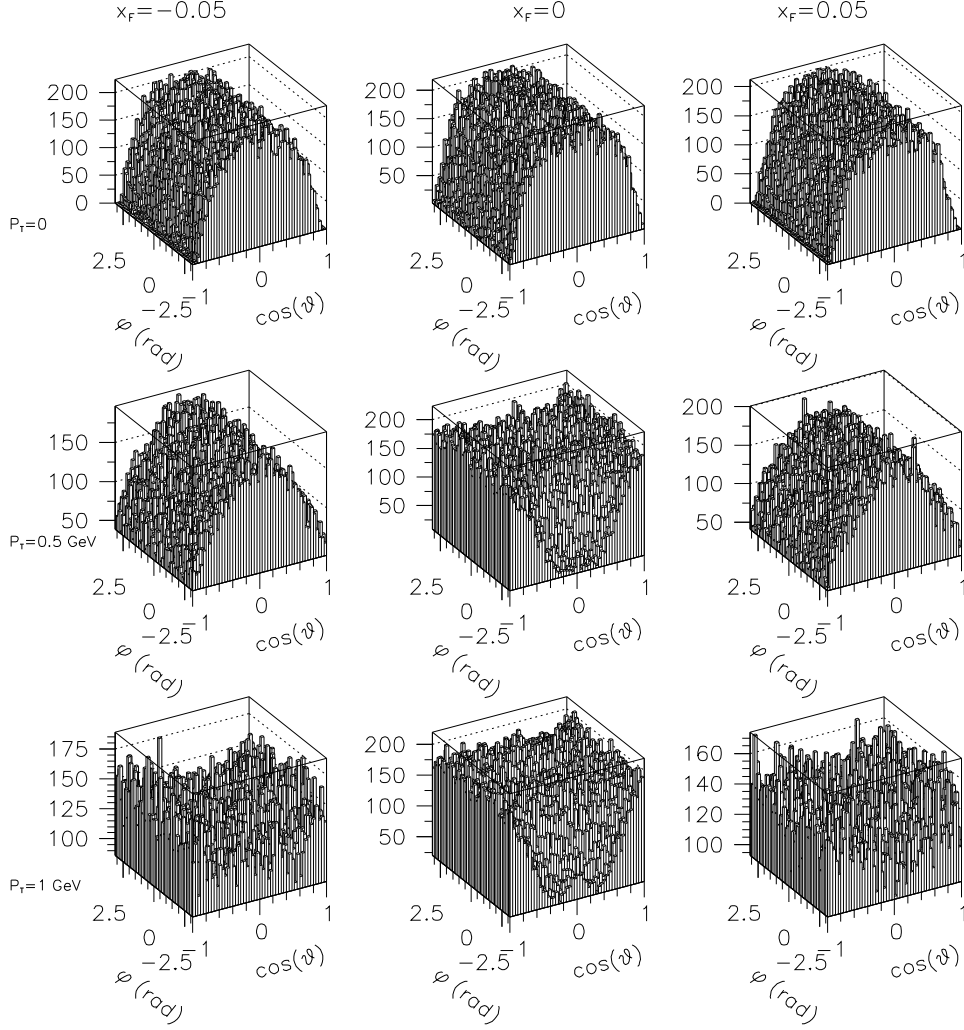


Figure 8: *LEGO* plots of the $\cos(\theta) - \phi$ geometric acceptance (not normalized) for a system with mass 2.5 GeV decaying in $\eta^0\eta^0 \rightarrow 4\gamma$. The nine plots shown are for the different combinations of $x_F = -0.05, 0.0, +0.05$ and $P_t = 0.0, 0.5, 1.0 \text{ GeV}$ values of the dipion system in the overall center-of-mass.

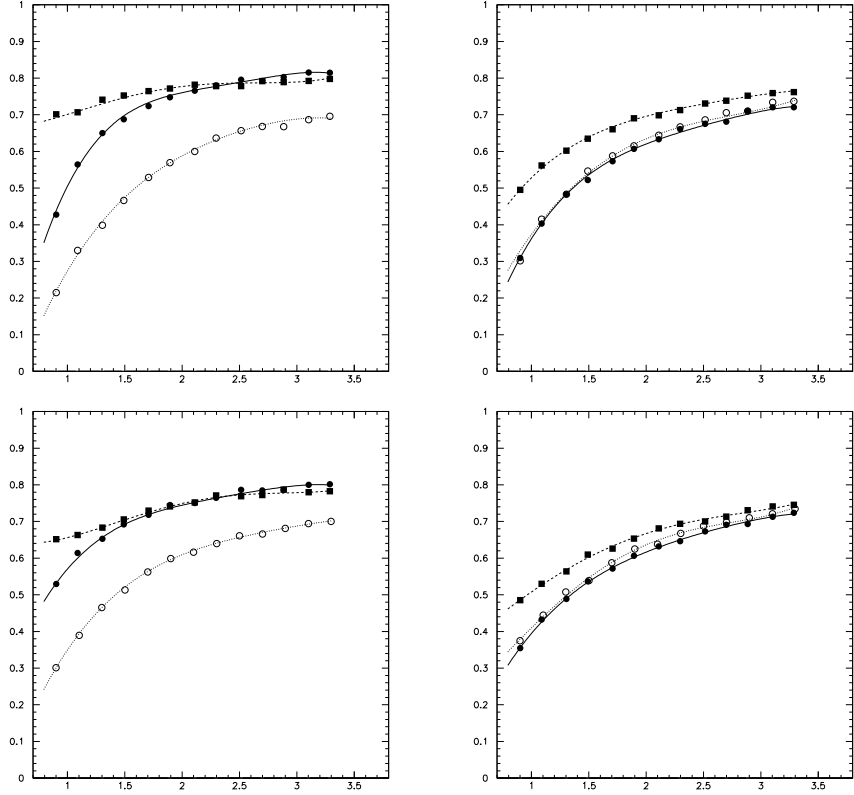


Figure 9: Geometrical acceptance as a function of the final state mass (in GeV) as obtained by the fast Monte Carlo simulation. Upper plots: Left is geometrical acceptance at $P_t = 0$ for $\pi^+\pi^-$; Right for $\pi^0\pi^0$. Solid squares for $x_F = 0$. Solid (open) circles for $x_F = -0.04$ ($+0.04$). Lower plots: same, but for $P_t = 0.5$ GeV.

RICH Interaction trigger				
Target Station	Wire Material	Total Stat. (million of events)	Reco. $\pi^0\pi^0$	Reco. $\pi^+\pi^-$
1 (b1)	Carbon	59.3	468	1524
1 (i1)	Tungsten	41.3	198	483
2 (b2)	Titanium	20.2	106	378
2 (i2)	Carbon	-	-	-
Total		120.8	772	2385
ECAL Interaction trigger				
Target Station	Wire Material	Total Stat. (million of events)	Reco. $\pi^0\pi^0$	Reco. $\pi^+\pi^-$
1 (b1)	Carbon	5.7	128	333
1 (i1)	Tungsten	-	-	-
2 (b2)	Titanium	-	-	-
2 (i2)	Carbon	66.5	2000	2867
Total		72.2	2128	3200

Table 3: *Summary of the total statistics of fully reconstructed events acquired during the 2002/2003 data taking and usable for the studies presented in this document. The number of reconstructed centrally produced $\pi^0\pi^0$ and $\pi^+\pi^-$ final states is also reported.*

6 Extracting DPE events from 2002-2003 minimum-bias data

During the 2002-2003 HERA-*B* data acquisition period when the priority was to collect as many inclusive J/Ψ events as possible on different nuclear targets, a large sample of minimum bias or interaction trigger events were also acquired for calibration purposes and for some inclusive hadron measurements. The trigger configuration used for these last studies were the following:

- RICH Interaction trigger: a minimum number of 20 hits in the RICH detector or a total energy in the inner ECAL greater than 1 *GeV* were asked at the Level-2.
- ECAL Interaction trigger: the ECAL pretrigger was acting as an interaction trigger at the Level-1 by requiring at least an electromagnetic cluster having transverse energy $E_T > 0.15$ *GeV* in an event. At the Level-2 events were selected having a maximum number of hits in the RICH less than 300 (corresponding to a maximum number of charged tracks of 8) and a number of reconstructed electromagnetic clusters with $E_T > 0.3$ *GeV* greater than 0 and less than 11.

The second trigger configuration was adopted in order to enhance the sample of events with low multiplicity of tracks and cluster typical of the events produced in DPE.

The summary of the acquired and fully reconstructed data sample used for the analysis presented in this document is shown in Table 3. In this Table the samples of data are classified depending on the interaction trigger used and on the target wire. From this Table we see that about 120 million such events were obtained using the RICH interaction trigger, and 70 million additional events were obtained using the ECAL interaction trigger. From these data, we isolated low-multiplicity final states which are fully contained in the spectrometer aperture and have the characteristics of centrally-produced systems with rapidity-gaps at small angle outside the spectrometer aperture. The last two columns of

Table 3 report the number of fully reconstructed $\pi^0\pi^0$ and $\pi^+\pi^-$, selected with the above mentioned criteria; if we calculate the number of reconstructed event per each triggered event, from the same Table, it is evident that the ECAL interaction trigger enhances the number of $\pi^0\pi^0$ relative to the number of $\pi^+\pi^-$ the latter being nevertheless triggered due to the non-negligible probability of hadrons showering in ECAL (about 30% for single hadron track).

For a better understanding of the following arguments presented in this proposal, we must anticipate here that, from the studies performed on the sample of events acquired, we conclude that the preferred running condition for HERA-*g* will be with ECAL interaction trigger and rapidity gap vetoing at the Level-1. Therefore for our rate estimates (see Section 7.2) and for all the arguments related to this item we will use only the sample of fully reconstructed events acquired with the ECAL interaction trigger. For the analysis of different final states presented in the following we will in general use (unless otherwise stated) the full data sample (ECAL and RICH interaction trigger and all the target wires).

6.1 Selection program

A selection program has been developed to select the topology of interesting events in central production. It is important to remember that these events are characterized by having only the produced final state in the detector and ideally nothing elsewhere (in the so called rapidity gaps).

The purpose of this selection is to cleanly define the final state both for charged and neutral final states. The selection program classifies the reconstructed track or electromagnetic cluster into five categories:

1. CHARGED TRACKS: reconstructed tracks (or segments of tracks) which originate in the vertex detector before the magnet and do not have electromagnetic clusters associated.
2. CHARGED CLUSTERS:reconstructed tracks (or segments of tracks) which originate in the vertex detector before the magnet and have one electromagnetic cluster associated.
3. NEUTRAL CLUSTERS: clusters detected in the ECAL with no track segments pointing to them.
4. NEUTRAL CLUSTERS WITH SINGLE CONVERSION:clusters detected in the ECAL with one track segment originating after the magnet pointing to them.
5. NEUTRAL CLUSTERS WITH MULTIPLE CONVERSIONS:clusters detected in the ECAL with more than one track segment originating after the magnet pointing to them.

All the events containing reconstructed tracks or clusters which do not belong to one of these categories (for example tracks originating in the magnet) are rejected. The categories 1) and 2) define a reconstructed *TRACK*, while the remaining ones define a *CLUSTER*. The categories 4) and 5) have been introduced to take into account photon conversions after the magnet.

The selection program is based on the global event reconstruction program of the HERA-*B* experiment which is not optimized for the reconstruction of centrally produced events. For example, it could happen that not all the available hits in the tracking systems are used in the event reconstruction, because a matching between a track segment reconstructed in the vertex system and in the main tracking systems is not found. This

is a potential source of background.

Studies have been performed in order to improve the performance of the global event reconstruction program. The possibility to extend the vertex detector acceptance up to a polar angle $\theta \sim 0.4$ radians has been investigated. By assuming the event vertex position, hits in the VDS were searched possibly clustering into a reconstructable track segment. The algorithm was tested by means of Monte Carlo generated events with the aim to maximize the reconstruction efficiency for $\theta < 0.4$ radians while keeping the probability of track misidentification at an acceptable level. This algorithm will be used in the near future to clean the sample of selected centrally produced events.

In our analysis we applied the selection code to a sample of about 120 million of events acquired with the RICH interaction trigger and of about 75 million of events acquired with the ECAL interaction trigger by requiring events having a number of reconstructed *TRACKs* less than six and (or) a number of reconstructed *CLUSTERs* less than eleven. Table 4 displays the multiplicity distributions for *TRACKs* and *CLUSTERs* of the complete data sample in hand, after rapidity-gaps were imposed offline and events were excluded which contained any evidence for particles other than those reconstructed by the full tracker.

# of <i>CLUSTERs</i>	# of <i>TRACKs</i>					
	0	1	2	3	4	5
8	11	0	0	0	0	0
7	18	0	0	0	0	0
6	28	1	1	1	0	0
5	42	1	2	1	0	0
4	70	3	3	1	0	0
3	115	5	4	2	1	0
2	234	9	6	2	1	0
1	578	10	6	2	1	0
0	–	10	6	1	1	0

Table 4: *Numbers of events (rounded off to the nearest thousand) as a function of the number of CLUSTERs and the number of TRACKs after (preliminary) off-line rapidity-gap and cleanliness cuts are made. The number of events refers to both the RICH and the ECAL interaction trigger data samples.*

In the following sub-sections, we summarize the first (preliminary) results from the available data sample acquired with the ECAL and RICH interaction trigger. Some of the final states shown in the table are discussed in the following sections. We start with the dipion channels, $\pi^+\pi^-$ and $\pi^0\pi^0$ which are obtained from the coordinates (*#ofCLUSTERs* = 0, *#ofTRACKs* = 2) and (*#ofCLUSTERs* = 4, *#ofTRACKs* = 0), respectively, in the Table 4.

It is evident that, even with these low statistics, we have been able to obtain very valuable information on the prospects of a new data run with rapidity-gap vetoes in the Level-1 trigger. In Table 5 we report a comparison of the overall statistics of the WA-102 experiment in some centrally produced two body final states, and the presently available statistics presented in this proposal. With the HERA-*g* ECAL interaction trigger described in Sect. 3.2, the events presented in this proposal correspond to about 5 minutes

of data taking ⁸ (as explained in Section 7.2). Thus, a run of 100 hours with the rapidity-gap trigger will yield more than 1000 times the data samples shown in the last column of Table 5, enough to make fundamental contributions in many areas (see also the summary Table 8 on the statistics achievable by HERA-*g* in other final states in Section 9.9).

Final State	WA-102 Statistics	Total Available Stat.	ECAL int. trigger. Stat.
$\pi^0\pi^0$ [1]	$\sim 1.7 \cdot 10^5$	2900	2128
$\pi^+\pi^-$ [14]	$\sim 2.9 \cdot 10^6$	5585	3200
K^+K^- [15]	$\sim 31 \cdot 10^3$	217	153

Table 5: Comparison of the overall statistics of the WA-102 experiment in some centrally produced two body final states, and the presently available statistics presented in this proposal.

6.2 Central $\pi^+\pi^-$ and $\pi^0\pi^0$ systems

For $\pi^+\pi^-$ central systems, we require two oppositely-charged tracks with at least 4 hits in the silicon system and at least 4 hits in the downstream tracking system. Standard quality cuts were applied to the reconstructed tracks and their vertices at a target wire. The selected $\pi^+\pi^-$ events are required to have no clusters in the ECAL (unless they are pointed to by the tracks since showering hadrons can leave substantial energy in the ECAL). The number of hits in the RICH counter for each track must be fewer than 35 (the maximum for one track). No further RICH selection is made on those events interpreted to be $\pi^+\pi^-$. About 5,500 $\pi^+\pi^-$ events are selected, 3200 from the ECAL interaction trigger and 2300 from the RICH interaction trigger. The invariant mass distribution is shown in Fig. 11 (left plot, solid line). The main features of the invariant mass distribution are an evident $f_2(1270)$ signal and a sharp drop at 1 GeV (probably due to the interference of the $f_0(980)$ with the S-wave background [14]).

The event selection for $\pi^0\pi^0 \rightarrow 4\gamma$ requires only 4 γ in the calorimeter and no reconstructed tracks originating in the silicon vertex system. For this analysis we use only the *NEUTRAL CLUSTERS* class of events defined in Section 6.1.

Figure 10 is a LEGO plot of paired $\gamma\gamma$ invariant Masses which shows the clean $\pi^0\pi^0$ signal. 2900 $\pi^0\pi^0$ events are selected, about 2100 from the ECAL interaction trigger and about 800 from the Rich interaction trigger. The invariant mass distribution is shown in Fig. 11 (right plot, solid line). The main features of the invariant mass distribution are again an evident $f_2(1270)$ signal and a sharp drop [1] at 1 GeV.

Figure 11 displays the complete observed mass spectra, uncorrected for acceptance losses, for both $\pi^+\pi^-$ (left) and $\pi^0\pi^0$ (right). The dotted histogram on each plot is the DPE prediction for $d\sigma/dM_X$ from UA8 [10], as discussed above in Sect. 4. The predictions shown are modified slightly from the 920 GeV curve in Fig. 6 to account for a decrease in the ratio, (2 pions/all final states), as M_X increases.

Because of the dominance of resonances for $M_X < 1.5$ GeV, which complicates the predictive powers of Eqn. 3, the prediction curves in Fig. 11 are normalized to the data with $M_X > 1.5$ GeV. Although the data have been not corrected for acceptance losses,

⁸A sample of about 120 million of RICH interaction triggers (see Sect. 3.2) was also acquired in 2002/2003 data taking. These data were most of the times summed to the ECAL interaction trigger data sample to produce the plots shown in the following of this document. Nevertheless, due to the fact that the trigger configuration proposed will be the ECAL interaction trigger one, all our extrapolations of the achievable statistics for HERA-*g* will be based on the latter trigger configuration.

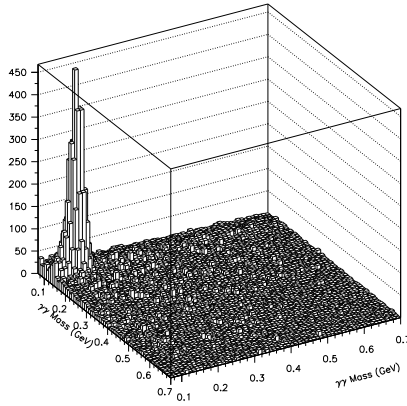


Figure 10: *LEGO plot of paired π^0 invariant masses used in selecting $\pi^0\pi^0$ events.*

Fig. 9 shows that the acceptance at $x_F = 0$, where most of the data are, changes very little above $M_X = 1.5$ GeV.

The agreement in shape between data and prediction seen in Fig. 11 is one of the supports of the hypothesis that the $\pi^+\pi^-$ and $\pi^0\pi^0$ channels are dominated by Double-Pomeron-Exchange. The 450 GeV curve in Fig. 6 has been found to agree (not shown here) with the WA-102 data on these channels. This gives us further confidence that the advantage of 920 GeV data for studying the high mass region implied by the numbers in Table 1 is reliable.

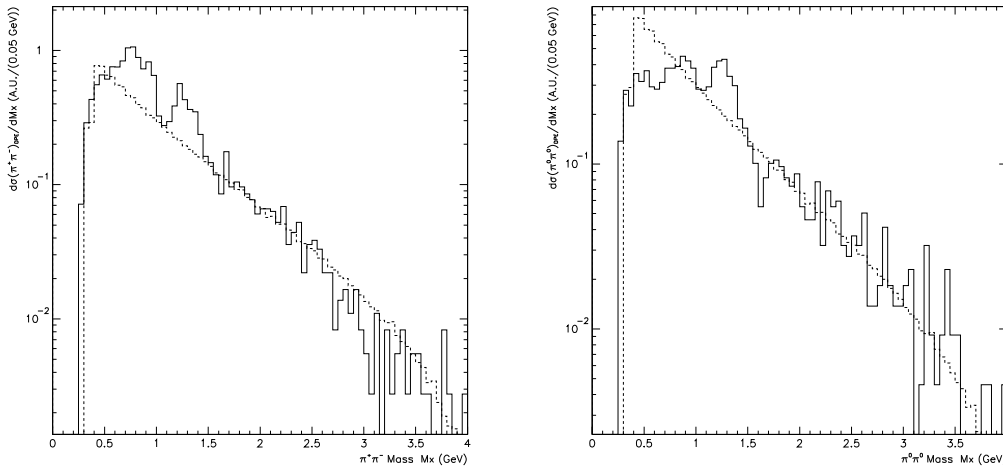


Figure 11: *Semi-log mass plots: Left-hand figure: Invariant mass of $\pi^+\pi^-$ final state; Right-hand figure: Invariant mass of $\pi^0\pi^0$ final state. Both are raw data. The dotted histograms are DPE predictions described in the text; they are normalized to the data for $M_X > 1.5$ GeV.*

Figure 12 shows a comparison between our relatively small data samples of $\pi^+\pi^-$ and $\pi^0\pi^0$ and published mass spectra from the WA-102 experiment. Because the experimental acceptances are different at low mass due to the beam-pipe imposed minimum-angle acceptance in the HERA-B detector, the figure shows the data for $M_X > 800$ MeV (where the acceptance is roughly constant for both the final states as shown in Table 2). The WA-102 data are normalized to the HERA-B data at the position of the 3-bin wide dip between the well-known falloff at 1 GeV and the beginning of the $f_2(1270)$ peak. The

WA-102 data sample was $\sim 1.7 \cdot 10^5$ events for the $\pi^0\pi^0$ [1] and $\sim 2.9 \cdot 10^6$ events for the $\pi^+\pi^-$ [14] final state; the plots for HERA-B are relative to the ECAL interaction trigger data set and contain $\sim 2.1 \cdot 10^3$ and $\sim 3.2 \cdot 10^3$ fully reconstructed events respectively.

We see that our $f(1270)$ signals seem to have improved resolution over WA-102. And, as expected (see Table 1), we have more events at larger mass. The WA-102 distributions stop at $M_X = 2.2$ GeV. We can conclude that we can carry out a phase shift analysis for mass between 1.5 and 3.0 GeV which should go far beyond what WA-102 was able to accomplish.

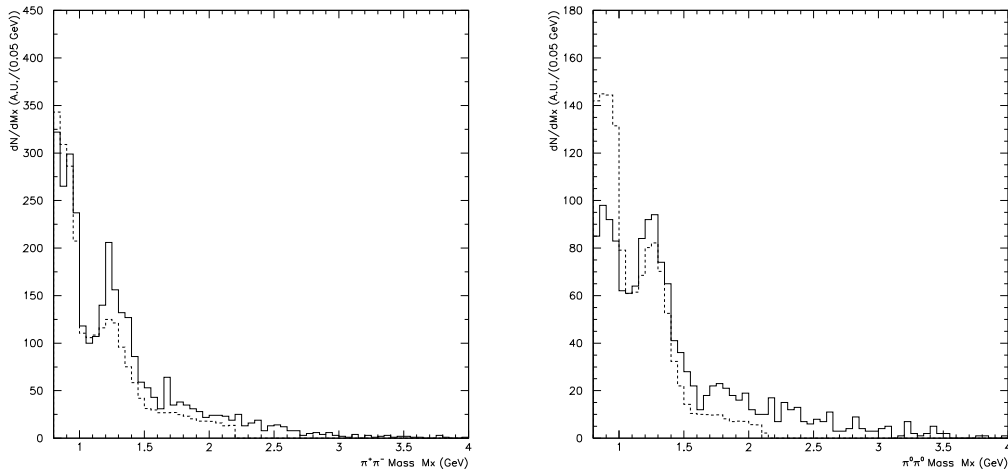


Figure 12: *Left-hand figure: Invariant mass of $\pi^+\pi^-$ final state; Right-hand figure: Invariant mass of $\pi^0\pi^0$ final state. Both are raw data. The dashed data are published WA-102 data, normalized to our data at the position of the 3-bin minimum between the falloff at 1 GeV and the low side of the $f(1270)$.*

6.3 Nuclear effects

Figures 13 (Left and Right) show the observed x_F distributions of $\pi^+\pi^-$ systems in the overall center-of-mass for data from Tungsten and Carbon wire targets, respectively. We see sharply peaked distributions with mean values that are slightly shifted to the positive side of 0. Although the distributions in Fig. 13 have not been corrected for acceptance losses, we saw in Sect. 5 that the acceptance for $\pi^+\pi^-$ at positive x_F is somewhat smaller than at negative x_F . Thus, acceptance corrections would exaggerate even more the asymmetry with respect to $x_F = 0$ seen in Figs. 13. If we had real proton-proton interactions, the symmetry of the initial state guarantees that x_F distributions must be symmetric around 0. Thus, our observed asymmetry must be a nuclear physics effect. Because of the dominance of Double- \mathcal{P} omeron-Exchange in this reaction, the asymmetry may be a consequence of an effectively smaller average \mathcal{P} omeron momentum in the nuclear target than in the beam proton. There could be some collective nuclear effects which are responsible for this. In any case, we need additional data and further study of this effect before drawing firm conclusions.

We note that the mean values of the two distributions in Fig. 13 are different; the mean values for W and C, respectively, are:

$$\langle x_F \rangle_W = 0.0147 \pm 0.0011 \quad , \quad \langle x_F \rangle_C = 0.0111 \pm 0.0006 . \quad (6)$$

An accurate estimate of systematic effects on the acceptance losses has yet to be performed (the C and W wires belong to the same station, but beam position asymmetries could

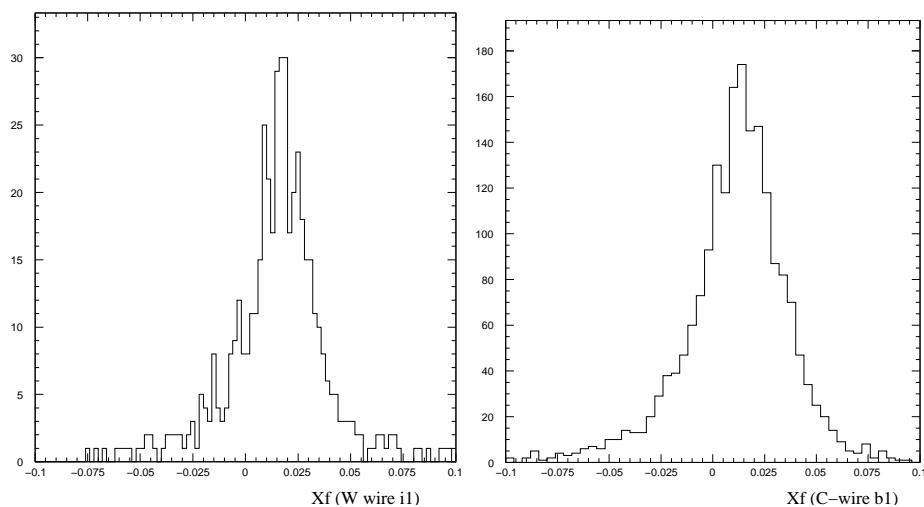


Figure 13: *Left: x_F distribution for $\pi^+\pi^-$ on Tungsten target wire. Right: x_F distribution for $\pi^+\pi^-$ on Carbon target wire. The data are uncorrected for acceptance losses and were taken with the RICH interaction trigger. The horizontal scales run from -0.1 to $+0.1$*

play a role). The $\pi^0\pi^0$ final state, should be less sensitive to beam position asymmetries due to the fact that the measured final state is formed only by neutrals which are not measured in the VDS. Unfortunately, the lower statistics available for the $\pi^0\pi^0$ final state, does not allow to confirm the effect of Eqn. 6 with statistical significance.

We plan to investigate this argument in more detail in the near future since the observed 3σ difference between the two mean values, shown in Eqn. 6 seems to say that the asymmetry effect in the x_F distribution is larger in Tungsten than in Carbon.

We return now to the discussion of Sect. 4 concerning the possibility of using the Pomeron flux factors to predict the shapes of observed x_F distributions. Eqn. 3 and Fig. 5 allow us to see that, at larger masses, the x_F peak should be broader than at lower masses. The Fig. 14 shows the observed x_F distribution for $\pi^+\pi^-$ when $M_X > 1.5$ GeV (to avoid the region at lower mass which is dominated by large resonance production). The superimposed histogram is a Monte-Carlo prediction generated using Eqn. 3. Since this equation is only valid at low values of $|t|$, we also apply the selection $P_t^2 < 0.3$ GeV² to the data. There is seen to be a reasonable agreement between data and prediction. One significance of this particular analysis is that it will lead to a greater understanding of Pomeron phenomenology. Some departures from predictions of this type will arise from Reggeon-Exchange or Odderon-Exchange.

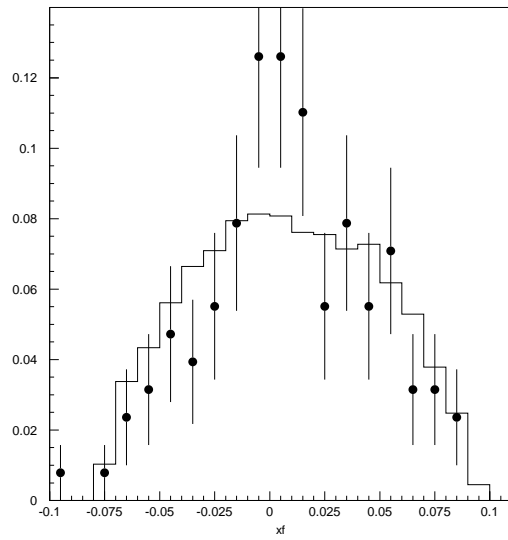


Figure 14: x_F distribution for $\pi^+\pi^-$ with $M > 1.5 \text{ GeV}$ and $P_t^2 < 0.3 \text{ GeV}^2$. Histogram is prediction using UA8 Pomeron flux factors as described in the text. The horizontal scale runs from -0.1 to $+0.1$

7 Monte Carlo simulations of inelastic events

We generated and reconstructed a substantial (few million event) sample of Monte Carlo inelastic events for each target wire used in the data-taking run. The generation was performed with the inelastic event generator and the reconstruction was based on our full detector description. This sample of Monte Carlo generated data is useful for the following purposes:

- to evaluate the suppression of inelastic events achievable with the proposed rapidity gap vetoing system;
- to predict the production rates for some centrally produced final states.

These topics will be treated in detail in the following sections.

7.1 Inelastic background suppression by means of rapidity gap vetoing system

As already mentioned (see Sect. 3.3), the HERA-*g* trigger will rely on a Level-1 scheme based on the ECAL interaction trigger and on rapidity gap vetoing (see Sect. 3.3). The latter will be given by the already installed Small Angle scintillator Counters (SAC) placed just behind the ECAL, and by Large Angle scintillator Counters (LAC), a scintillator system that will replace the first station of the existing VDS.

The actual Monte Carlo detector geometry developed for the HERA-*B* experiment does not include these two detectors. In order to study the suppression on inelastic events achievable for HERA-*g* we have therefore developed a simplified model. This model consists of using the momentum vectors of all the Monte Carlo generated charged particles (and gammas) which originate from the primary vertex to extrapolate to the geometrical position of the SAC and LAC. In order to check the validity of this model we used the available data from the SAC.

In Fig. 15 we show the SAC suppression for inelastic events versus efficiency as measured for the RICH interaction trigger (upper points) and for the ECAL interaction trigger (inclusive of Level-2 algorithm, lower points). The efficiency is measured with respect to the HERA machine empty bunches (i.e. the probability to classify an empty bunch as empty). The inelastic suppression is instead measured with respect to all the triggered events. The different points are obtained by changing the threshold of the SAC. In all our analysis we used a threshold value for the SAC corresponding to an efficiency of 90%.

In Fig. 16 we show the results of a Monte Carlo study of trigger suppression for centrally produced events in the 2002/2003 data taking configuration (where the SAC suppression can be evaluated only by off-line analysis). The numbers in this figure are normalized to the total number of interactions. The effect of SAC suppression is obtained, using the model described above, by vetoing the events with one or more charged tracks crossing the SAC geometric cross section.

From this simple model we can estimate that the SAC suppression is a factor of ~ 9 for the RICH interaction trigger data (upper plot of Fig. 16) and ~ 6 for the ECAL interaction trigger data (lower plot in the same Figure). Comparing these results to Fig. 15 we can see that the obtained values are in a 10% (20%) agreement with the values obtained from real data for the RICH (ECAL) interaction trigger for an estimated efficiency value of about 90%.

The model adopted for the simulation of the SAC gives suppression factors in reasonable agreement with the measured ones, and therefore we will use it (and assume it holds also for LAC suppression) in the next section for the evaluation of the expected HERA-*g*

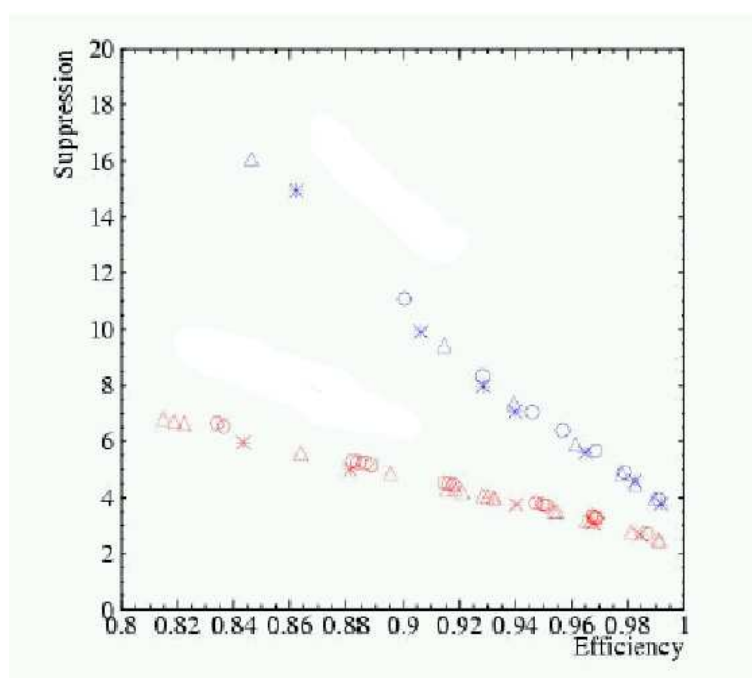


Figure 15: *The SAC inelastic suppression versus efficiency. Upper points: RICH interaction trigger. Lower points: ECAL interaction trigger.*

production rates for centrally produced $\pi^+\pi^-$ and $\pi^0\pi^0$ final states.

The effect of the LAC suppression, evaluated from the same Monte Carlo data sample, is shown in Fig. 17; here the suppression on inelastic due to the combined action of the SAC and the LAC is plotted as a function of the maximum LAC coverage angle θ_{MAX} (polar angle in the laboratory system). Two cases of minimal LAC coverage angle θ_{MIN} are shown: $\theta_{MIN} = 0.25 \text{ rad}$ (circles) and $\theta_{MIN} = 0.20 \text{ rad}$ (squares). One can see that the needed global factor of 100 of inelastic suppression at Level-1 can be obtained by vetoing up to $\theta_{MAX} \simeq 0.9 \div 1.0 \text{ rad}$.

In Fig. 18 we report the results for the Monte Carlo simulation of the suppression of inelastic events for the trigger scheme proposed for HERA-*g*. From this figure we can see that choosing the LAC configuration with the large solid angle coverage, the rapidity-gap vetoing obtained by a logical “OR” of the SAC and LAC signals at Level-1 will provide a factor 100 in suppression of the inelastic background. In the same figure the factor of two suppression presently obtainable at the Level-2 (with a modified algorithm with respect to the 2002/2003 data taking, as will be explained in the following section) is also shown.

7.2 HERA-*g* rates for centrally produced final states

The data acquired with the ECAL interaction trigger by HERA-*B* during 2002/2003 running, together with the Monte Carlo inelastic data sample generated with the full detector geometry, allow us to make a solid prediction of the rates for centrally produced final states of HERA-*g*.

In the first five rows of Table 6, we summarize the expected rates for HERA-*g* using a Carbon target at 1 *MHz* interaction rate⁹. The first two columns of this table report the rates of the 2002/2003 data taking after each of the cuts applied at Level-1 and Level-2,

⁹The presence of an efficient rapidity gap vetoing system could allow us to work to higher interaction rates, so increasing the achievable statistics

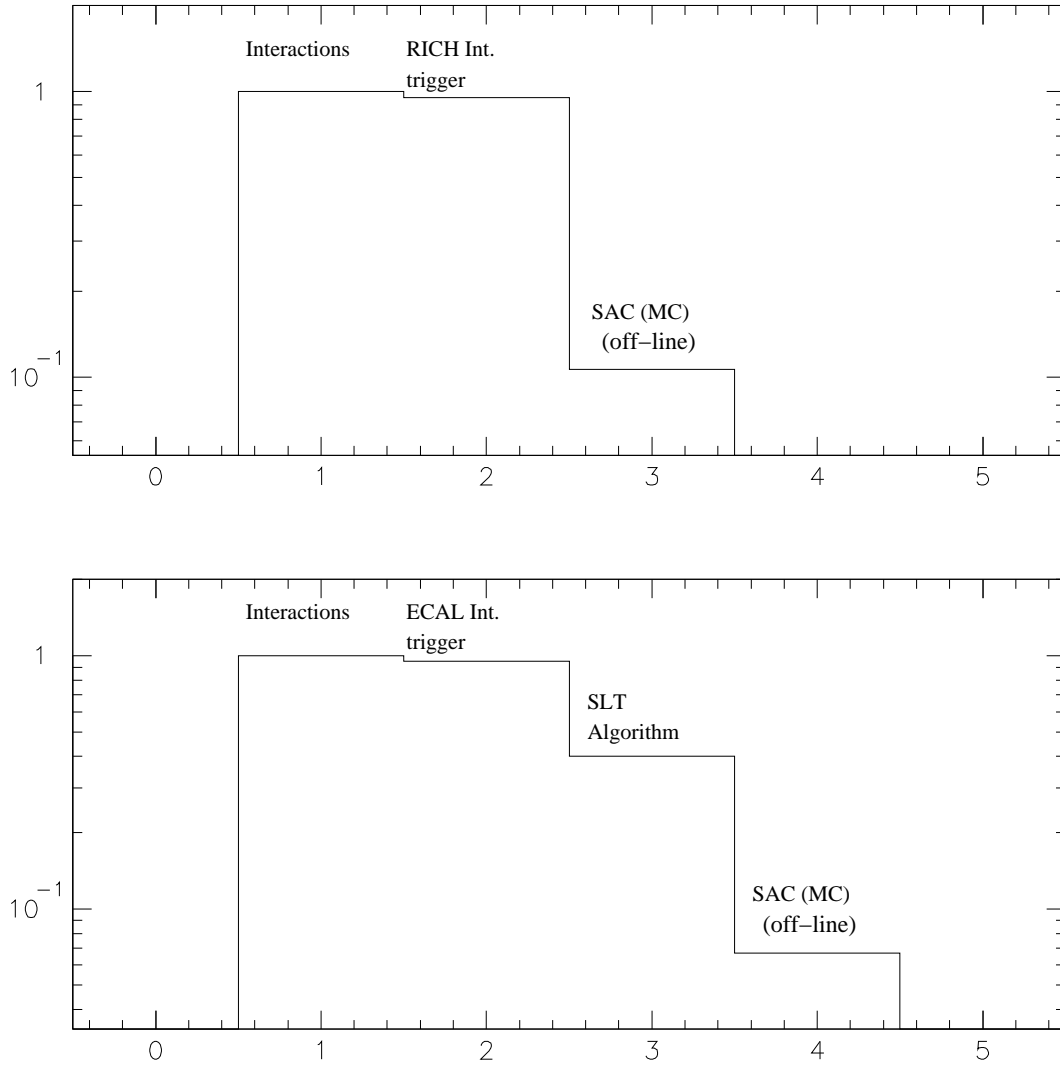


Figure 16: Monte Carlo simulation of the suppression of inelastic events for the trigger schemes adopted in 2002/2003 data taking for selection of centrally produced events. Upper: RICH interaction trigger. Lower: ECAL Interaction trigger. Numbers are normalized to the total number of interactions.

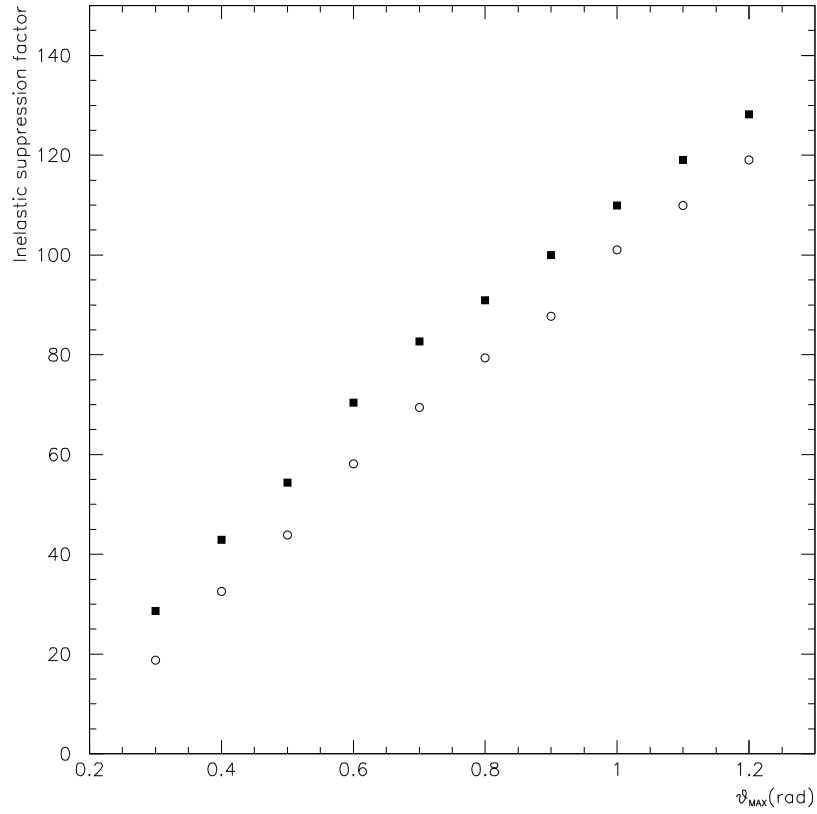


Figure 17: *SAC and LAC inelastic suppression as a function of the maximum LAC coverage angle θ_{MAX} (polar angle in the laboratory system). Circles: Minimal LAC coverage angle $\theta_{MIN} = 0.25$ rad. Squares: Minimal LAC coverage angle $\theta_{MIN} = 0.2$ rad.*

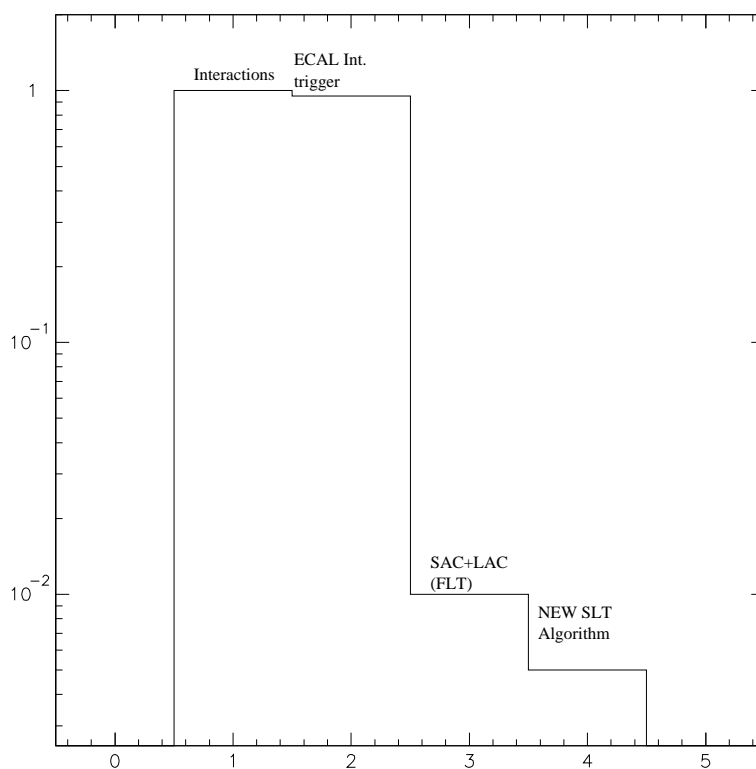


Figure 18: *Monte Carlo simulation of the suppression of inelastic events for the trigger scheme proposed for HERA-g . Numbers are normalized to the total number of interactions.*

and the last two columns give the rates for HERA-g . The suppression factors associated with each cut are for the 2002/2003 run and were already reported already in Fig. 16 (lower plot), and for HERA-g , in Fig. 18.

In the HERA-B and the HERA-g DAQ scheme the main limiting factors to the achievable rate are the Level-2 maximum input rate (10 kHz) and the maximum logging rate (1 kHz). These limitations cost a factor of ~ 400 (prescaling factor ~ 100 at the Level-1 and ~ 4 at the Level-2) on the achievable signal for centrally produced events during the 2002/2003 run, as can be seen from the *Prescaling* rows of Table 6. The factor of loss in the statistics achievable for centrally produced events is expressed by the quantity F_{lt} (live time fraction) defined as the percentage of time that the acquisition is live to acquire these events.

More generally:

$$R_{final\ state}(HERA-g) = R_{final\ state}(HERA-B) \cdot \frac{F_{lt}(HERA-g)}{F_{lt}(HERA-B)} \quad (7)$$

and,

$$M_f = \frac{T(HERA-g) \cdot F_{lt}(HERA-g)}{T(HERA-B) \cdot F_{lt}(HERA-B)} \quad (8)$$

Eqn. 7 can be used to calculate the expected rate in HERA-g for a centrally produced final state starting from the measured rate of fully reconstructed events in 2002/2003 for the same channel. Eqn. 8 expresses the multiplication factor for the statistics of centrally produced reconstructed events in the 2002/2003 sample as a function of the HERA-g running time , $T(HERA-g)$, and the live time fraction F_{lt} reported in Table 6 for HERA-B and HERA-g.

	Run 2002/2003		HERA- <i>g</i>
	Rate (Hz)		Rate (Hz)
Interaction	10^6	Interaction	10^6
Level-1	$0.95 \cdot 10^6$	Level-1	$0.95 \cdot 10^6$
Prescaling ($\frac{1}{100}$)	$\simeq 10^4$	Rap-gap Veto	$\leq 10^4$
Level-2 Algorithm	$4 \cdot 10^3$	New Level-2 Algorithm	$\leq 5 \cdot 10^3$
Prescaling ($\simeq \frac{1}{4}$)	$\simeq 10^3$	Further Level-2 improv. (or prescaling $\simeq \frac{1}{5}$)	$\simeq 10^3$
Logging rate	$\simeq 10^3$	Logging rate	$\simeq 10^3$
F_{lt} (live time fraction)	$\frac{1}{400}$	F_{lt} (live time fraction)	$\frac{1}{5} < F_{lt} < 1$

Table 6: Comparison of the rates between the 2002/2003 ECAL interaction trigger data taking and HERA-*g* as a function of the different cuts applied at the Level-1 and Level-2 trigger. The numbers refer to 1 s of data taking at 1 MHz interaction rate with Carbon wire. Units for quantities are Hz everywhere except for the dimensionless live time fraction.

Therefore, under the reasonable assumption that the Level-1 and Level-2 scheme adopted for HERA-*g* will not affect the signal efficiency, using the Eqn. 7, we can see that, for a dead-time free DAQ scheme the rate measured in 2002/2003 can be multiplied by a factor 400.

We will describe now the strategy to gain the factor 400 that was lost in the 2002/2003 data taking.

First, we note that the HERA-*g* rapidity gap vetoing system will reduce the inelastic interaction rate by a factor 100 according to the Monte Carlo simulation (see row *Rap-gap Veto* in the same table).

The remaining factor of 10 to reach an ideally dead-time free acquisition of centrally produced events, should therefore be gained at Level-2. During the 2002/2003 data taking, the Level-2 algorithm applied a cut on the maximum number of hits in the RICH detector and on the ECAL cluster multiplicity (see Sect. 6). The same algorithm will not give the needed suppression at Level-2 and must be modified and improved for HERA-*g*. In the estimate presented in row *New Level-2 Algorithm* of Table 6 we decreased, with respect to the Level-2 algorithm used in 2002/2003, the threshold on the transverse energy E_T of a reconstructed ECAL cluster from 0.3 GeV to 0.05 GeV (accepting up to ten clusters satisfying this condition) and reduced the upper limit of hits in the RICH detector from 300 (8 tracks) to 150 (4 tracks). This latter stricter condition does not significantly compromise the efficiency of any of the channels that HERA-*g* will study and gives a factor 2 of suppression at the Level-2. The missing factor of 5 can be gained by:

- improving the Level-1 scheme itself. Most probably some margin for gain in inelastic suppression is left by decreasing the LAC acceptance or by increasing the E_T threshold at trigger level while preserving the efficiency for the signal at the actual value;
- applying kinematical cuts at the Level-2 using the information of ECAL, RICH and part of the tracking system.

The details of the last two points will be developed in the near future. In the worst case, if we can not gain at the Level-2 a further factor ~ 5 , it will be possible to gain only

Final state Full Reco	Run 2002/2003	HERA- <i>g</i> $F_{lt} = \frac{1}{5}$	HERA- <i>g</i> $F_{lt} = 1$
$\pi^+\pi^-$	$4.4 \cdot 10^{-2}$	~ 3.5	~ 17.5
$\pi^0\pi^0$	$2.9 \cdot 10^{-2}$	~ 2.3	~ 11.5

Table 7: Comparison between the Run 2002/2003 and HERA-*g* logging rates (*Hz*), for the full reconstructed $\pi^+\pi^-$ and $\pi^0\pi^0$ final states.

a factor 80 in statistics with respect to 2002/2003 for the final states of interest.

Table 7 shows the acquisition rates of fully reconstructed $\pi^+\pi^-$ and $\pi^0\pi^0$ in the 2002/2003 run and their extrapolations to HERA-*g*¹⁰. The $\pi^+\pi^-$ and $\pi^0\pi^0$ rates for the 2002/2003 data can be obtained directly from Table 3 for the ECAL interaction trigger. In 2002/2003 the data were logged at 1 *kHz*, the total duration of the data taking (ECAL interaction trigger run) was $T(\text{HERA-}B) \sim 72200$ *s*, and the collected statistics ~ 72.2 millions of events. Therefore, from the ECAL interaction trigger section of Table 3, one can extract the rate of reconstructed $\pi^0\pi^0$ as $\frac{2128}{72200} \sim 0.029$ *Hz*, and of reconstructed $\pi^+\pi^-$ as $\frac{3200}{72200} \sim 0.044$ *Hz*. The minimum and maximum rate for HERA-*g* are obtained by multiplying the 2002/2003 rates respectively by a factor ~ 80 and ~ 400 (see Eqn. 8).

The numbers reported in Table 7 show the enormous potentiality of HERA-*g*. **By reasonably assuming the central value rates reported in the last two columns of Table 7 for HERA-*g*, and using Eqn.8, we see that in only 100 hours of data taking we could already achieve a statistics more than ten times higher than WA-102 for the $\pi^0\pi^0$ and about 30% higher for the $\pi^+\pi^-$ final states.** This would roughly correspond to a multiplication factor $M_f \sim 1000$ (Eqn.8) for the statistics (from data taken with ECAL interaction trigger) of all the final channels presented in this document (see also Table 8).

This means that already in a reasonably conservative scenario, in only 100 hours of data taking HERA-*g* could reach unprecedented statistics for centrally produced events.

¹⁰A more detailed survey, taking into account all the centrally produced final states presented in this proposal, on the expected statistics for HERA-*g*, will be presented in Table 8 of Section 9.9.

8 P_t^2 distributions and ϕ correlations

In addition to the invariant mass and x_F of centrally produced systems, there is an important third variable, namely the squared-transverse-momentum, P_t^2 , of the central system. In a Double- \mathcal{P} omeron-Exchange process, P_t^2 is the squared vector sum of the transverse momenta of the two exchanged \mathcal{P} omerons.

The importance of this observation is related to the important WA-102 result that the distribution in azimuthal angle between the two final-state protons in React. 1 displays striking correlations with the spin-parity of the centrally-produced system [11, 12, 13]. We note that a characteristic ϕ dependence predicts a specific P_t^2 dependence. It should therefore not be necessary to measure the final-state protons to use the WA-102 ϕ correlation effects to aid in spin-parity determination.

In Fig 19, the Left-hand plot shows our observed P_t^2 distribution for the complete $\pi^+\pi^-$ data sample for the range, $0 < P_t^2 < 1.0 \text{ GeV}^2$. The Middle and Right-hand plots

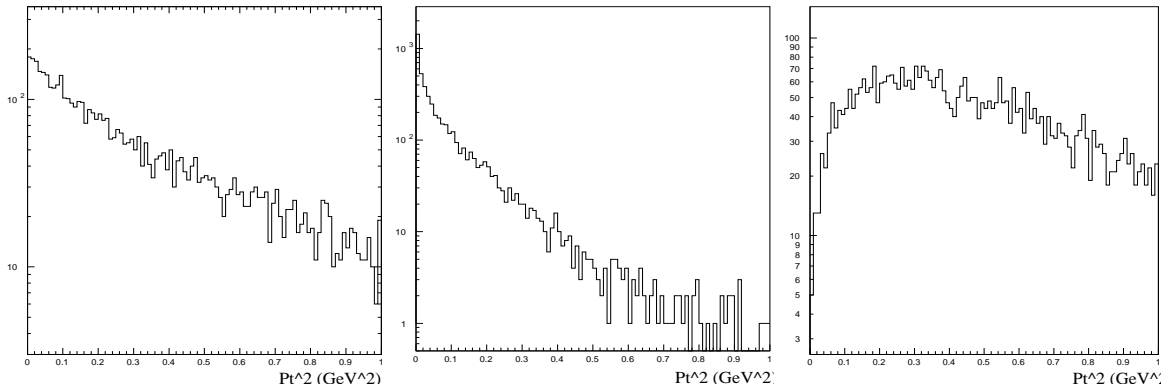


Figure 19: *Left: P_t^2 for $\pi^+\pi^-$ data; Center and Right are Monte-Carlo calculations for fixed ϕ between protons, 180° and 0° , respectively.*

correspond to a simple Monte-Carlo generation of two independent protons using the full \mathcal{P} omeron flux factor in Eq. 2. The transverse momenta of each is then calculated and, for the Middle plot, the azimuthal angle between the two protons is fixed at $\phi = 180^\circ$; for the Right-hand plot, it is fixed at $\phi = 0^\circ$. For 180° , the average transverse momentum cancels and we see a sharp peak at $P_t^2 = 0$, whereas for 0° , the transverse momenta add and we see a dip at $P_t^2 = 0$ with a large population at larger P_t^2 .

We also note that WA-102 finds that their glueball candidates tend to favor the case of $\phi = 0^\circ$, corresponding to larger P_t^2 values. According to WA-102, making such a cut should tend to enhance glueball signals. We postpone until Sect. 9.2 an illustration of two examples of P_t^2 distributions which result from two specific observed ϕ distributions which we actually use to resolve a spin-parity ambiguity of an observed signal.

9 Other channels, DPE or \mathcal{R} eggeon-Exchange

9.1 $K_s^0 K_s^0$ and $K^+ K^-$

$K_s^0 K_s^0$ events are selected from the data sample with four fully-reconstructed tracks with total charge zero. Track segments seen in the silicon vertex detector project into the downstream tracking system and satisfy our standard track-matching and vertexing procedure. Pairs of oppositely charged tracks were required to have a common vertex point downstream of a target wire. Figure 20 shows a LEGO plot of the two masses of such events. After applying the cuts, $0.48 < M(\pi^+ \pi^-) < 0.52$ GeV, the $K_s^0 K_s^0$ invariant mass of the 646 surviving events¹¹ is shown below in Fig. 21 Left.

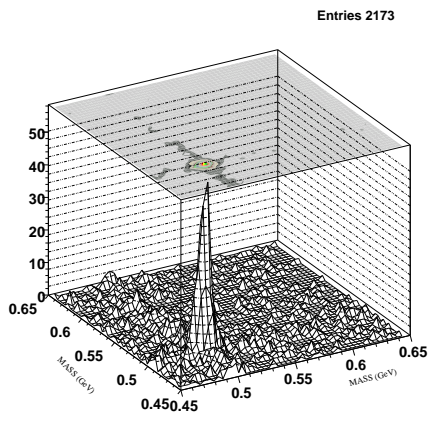


Figure 20: *Lego plot of $Mass_1(\pi^+ \pi^-)$ vs. $Mass_2(\pi^+ \pi^-)$ showing $K_s^0 K_s^0$ signal.*

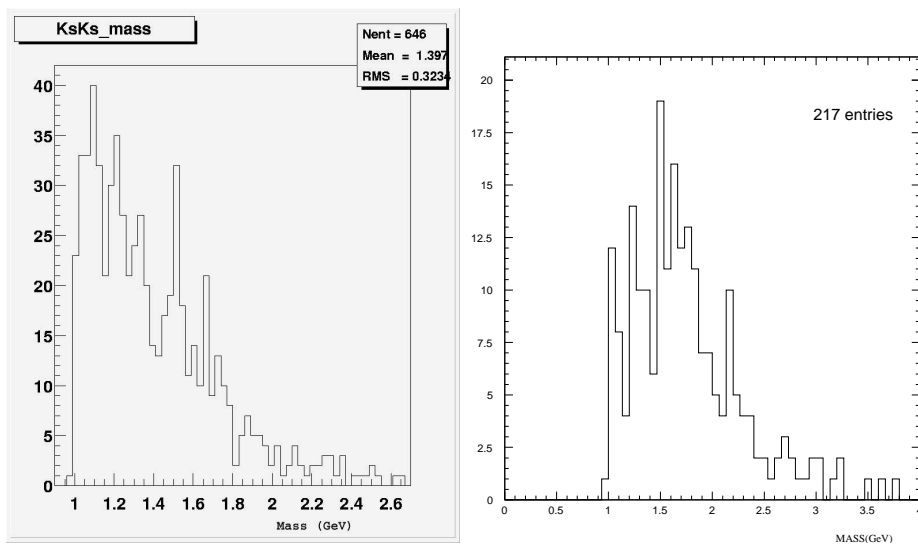


Figure 21: *Left: $K_s^0 K_s^0$ mass (646 events); Right: $K^+ K^-$ mass (217 events). The horizontal scales are in GeV units.*

¹¹In the present preliminary state of the analysis of this final state, the RICH interaction trigger data sample alone was used, and some important further cleaning is still required by applying the off-line SAC rapidity-gap vetoing and asking for no *CLUSTERS* (see Sect. 6.1) in ECAL. These cuts are estimated to reduce the present statistics by a factor ~ 30 . Nevertheless we consider useful to show the present results to illustrate the capability to reconstruct a sample of $K_s^0 K_s^0$ events.

The K^+K^- final state is selected from events with two oppositely-charged tracks. The RICH software furnishes likelihood values for each track for each particle type. Figure 21 Right shows the K^+K^- invariant mass spectrum for 217 events (153 of which comes from the ECAL interaction trigger) for which each track has a likelihood of being a kaon greater than 50%. The selected events sample for K^+K^- final state is 3.9% of the number of $\pi^+\pi^-$ events. In both $K_s^0K_s^0$ and K^+K^- spectra, there are good hints for considerable structure which will be clarified with the enormous statistics which will be available to us. In the K^+K^- invariant mass spectrum we can observe an enhancement of signals at threshold (in the region mass of the $\phi(1020)$, but also S-wave interference between $a_0(980)$ and $f_0(980)$), in the regions around the $f_2(1270) / a_2(1320)$, the $f_0(1500)$, the $f_0(1710)$ and, maybe, around the $f_2(2150)$. In the $K_s^0K_s^0$ invariant mass spectrum, even with limits of the present analysis, a signal enhancement around the $f_2'(1525)$ can be seen.

9.2 $\eta\pi^+\pi^-$ in $2\gamma\pi^+\pi^-$ final state

We now consider the final state, $2\gamma\pi^+\pi^-$. Figure 22 Left shows the $\gamma\gamma$ invariant mass distribution. We see clean signals for π^0 and for η . The Right-hand figure shows

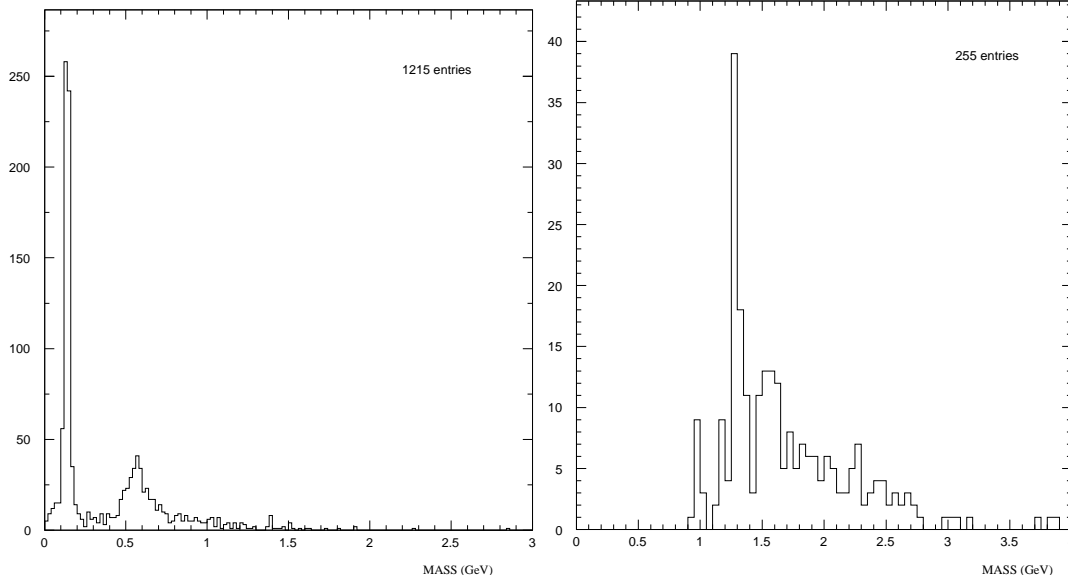


Figure 22: *Left: $\gamma\gamma$ mass spectrum (with selection for each γ , $P_t > 200$ MeV); Right: $\eta\pi^+\pi^-$ mass spectrum.*

the invariant mass for the $\eta\pi^+\pi^-$ system (255 reconstructed events, 185 coming from the ECAL interaction trigger data sample). Although there is a hint of a signal for the $\eta'(980)$, the prominent effect is a pronounced peak just below 1300 MeV (the highest bin has limits 1250-1300 MeV and there are 50 events between 1250-1350 MeV).

In the mass region of the peak, there are two known states with almost the same mass and width, but with different spin-parities [16]: the $\eta(1295)$ with $\Gamma = 55$ MeV and $J^{PC} = 0^{-+}$ and the $f_1(1285)$ with $\Gamma = 25$ MeV and $J^{PC} = 1^{++}$. We are able to discriminate between these two states because WA-102 has found that they have characteristically different azimuthal distributions between their protons. Fig. 23 shows these two ϕ distributions and their corresponding P_t^2 distributions obtained with the simple Monte-Carlo calculation referred to in Sect. 8.

From the bottom center of Fig. 23 we observe that the 50 events in the mass range 1250-1350 MeV have a P_t^2 distribution that resembles more closely the one for a $J^{PC} = 1^{++}$ than the one for a $J^{PC} = 0^{-+}$ final state. This fact is an indication that the peak observed in Fig. 22 Right is the $f_1(1285)$.

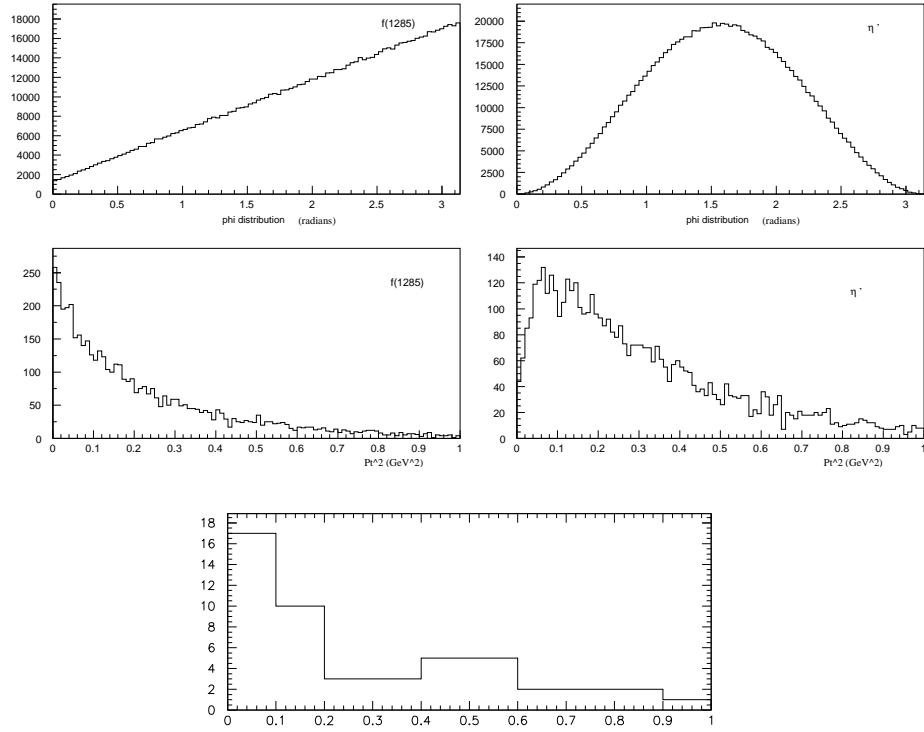


Figure 23: *Left side: ϕ distribution (upper) observed by WA-102 for $J^{PC} = 1^{++}$ and generated P_t^2 distribution (lower); Right side: Same for $J^{PC} = 0^{-+}$. Bottom center: Real data P_t^2 distribution for the events in the mass range $1250 \div 1350$ MeV for the $\eta\pi^+\pi^-$ final state.*

9.3 η and ω^0 in $2\gamma\pi^+\pi^-$ final state

In this section, we examine the events in the π^0 peak just seen in Fig. 22 Left. After removing the cut, $P_t > 200$ MeV, Fig. 24 shows the calculated $\pi^+\pi^-\pi^0$ mass distribution: The entire mass spectrum using 40 MeV mass bins is on the Left side of the figure; there

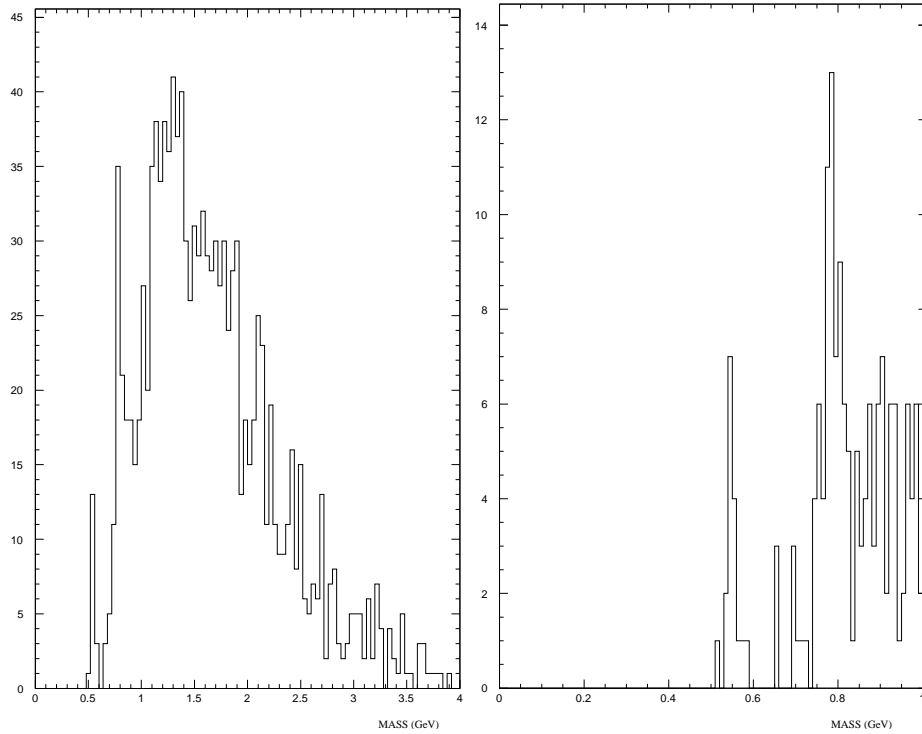


Figure 24: *Left side: $\pi^+\pi^-\pi^0$ mass spectrum (40 MeV mass bins); Right side: same with 10 MeV mass bins.*

are peaks at the positions of the $\eta(550)$ and the $\omega(782)$. The total spectrum consists of about 1300 events 900 of which coming from the ECAL interaction trigger data sample. Their mass region is shown expanded using 10 MeV bins on the Right-hand figure. We see that there are 15 events in the η peak with no background The ω peak is also quite clear with some background.

The interest in the ω is that if it is centrally-produced in isolation from other particles, its negative C-parity requires the exchange of a 3-gluon \mathcal{O} dderon. This is therefore a potentially very exciting area of study, if we can provide solid evidence for the existence of the \mathcal{O} dderon.

9.4 $\pi^+\pi^-\pi^+\pi^-$ in 4-track events

Figure 25 shows the invariant mass distribution for the final state, $\pi^+\pi^-\pi^+\pi^-$. A large

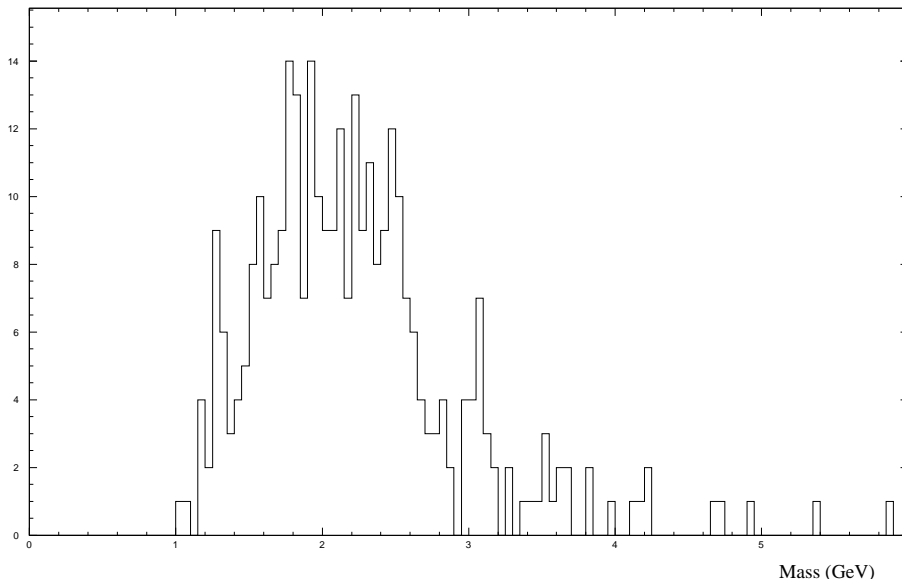


Figure 25: $\pi^+\pi^-\pi^+\pi^-$ mass spectrum.

increase in statistics for this state will be very welcome. The total statistics is 320 events (220 coming from the ECAL interaction trigger). There are potentially many interesting items in this mass spectrum.

First, we note that it begins at a mass of about 1 GeV with the main part of the distribution extending up to about 4 GeV.

We note a hint of a signal for the $f_1(1285)$ at a statistics level compatible with the size of its $\eta\pi^+\pi^-$ decay mode in Fig. 22. There is clearly a lot of other activity in this distribution, perhaps even near 3 GeV. The enhancement around 1.5 GeV is perhaps due to the $f_0(1450)$ (interference effect between the $f_0(1300)$ and $f_0(1500)$) quoted by [18].

One interesting physics possibility that could be studied in this channel is the possibility of “ \mathcal{P} omeron- \mathcal{P} omeron diffractive scattering. By this, we mean peripheral \mathcal{P} omeron- \mathcal{P} omeron scattering with a \mathcal{P} omeron-Exchange which might turn each incident \mathcal{P} omeron into a glueball [19]. Then we might have, for example, the process:

$$\mathcal{P}\mathcal{P} \rightarrow G(\pi^+\pi^-)G(\pi^+\pi^-). \quad (9)$$

One signature of this process would be polar structure of the type seen inclusively in React. 1 by the UA8 Collaboration [10]. Polar selection in the data might then enhance glueball signals in the individual $\pi^+\pi^-$ mass spectra.

9.5 $K_s^0 K^\pm \pi^\mp$ in 4-track events

Figure 26 shows the properties of another class of events which are obtained from the same 4-track data sample used for the $K_s^0 K_s^0$ events in Sect. 9.1. We now require that only one K_s^0 is found and that the remaining two tracks form a vertex at a target wire. RICH information is used to identify one of the two tracks as a K^\pm . These events correspond to the $K_s^0 K^\pm \pi^\mp$ final state, which can be used to search for the 0^{-+} $\eta(1440)$ state. If this state is found, it would be the highest mass 0^{-+} state observed in Double- \mathcal{P} omeron-Exchange and would open the way for the search for a 0^{-+} glueball in the 2 GeV region. The WA-102 experiment was unable to find any 0^{-+} states with higher mass than $\eta(550)$ and $\eta(980)$.

Figure 26 shows at the Left, the K_s^0 signal, and Center, the $K^\pm \pi^\mp$ mass distribution. A clear, but low statistics $K^*(890)$ signal is seen (with even a hint of events in the $K^*(1400)$ region). We select the events in the $K^*(890)$ region and show the $K_s^0 K^*$ mass in Fig. 26 Right (19 reconstructed events, 14 coming from the ECAL interaction trigger data sample). There is a cluster of events at threshold in $K_s^0 K^*$ which could be the $\eta(1440)$ or the $f_1(1440)$, but nothing more can be done with this study until additional statistics are available.

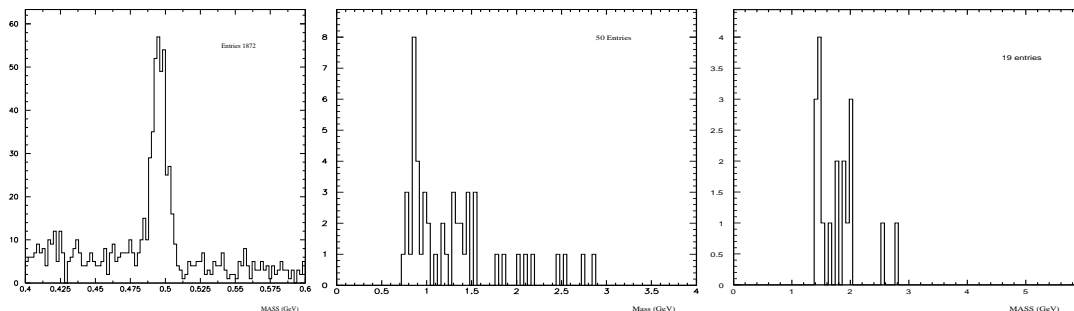


Figure 26: *Mass spectra: Left: $\pi^+\pi^-$, Middle: $K^\pm\pi^\mp$, Right: $K_s^0 K^\pm \pi^\mp$.*

Figure 27 repeats the Center and Right plots in Fig. 26 but without carrying out the particle identification on the K^\pm . Since any interesting signals in these events come from isolated states, and since we already have the K_s^0 identified, it is most likely that one of the charged tracks is also K^\pm . Therefore, we assign a K^\pm identification to the track with the largest momentum. We see in the Right part of the figure that the threshold enhancement is statistically enhanced. Its P_t^2 distribution should now be studied to see if we can identify the spin-parity as described in Sect. 9.2 for the $\eta\pi^+\pi^-$ final state.

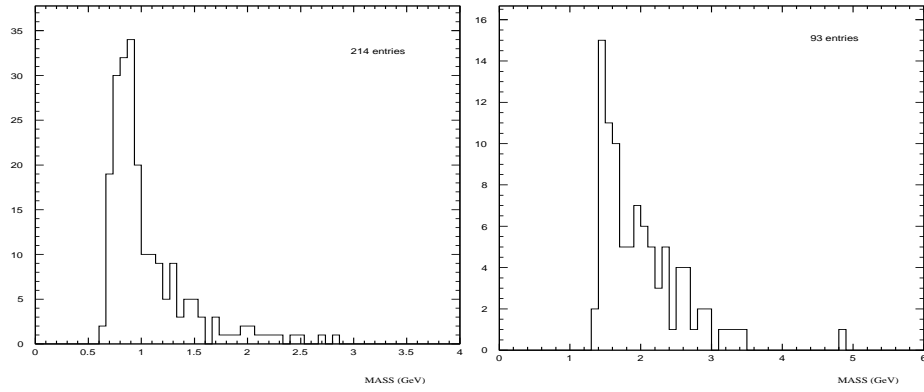


Figure 27: $K^\pm\pi^\mp$ and $K_s^0K^*$ mass distributions with no RICH identification of K^\pm . The track with the highest momentum is assumed to be the K^\pm

9.6 Hybrid search in \mathcal{P} omeron- \mathcal{R} eggeon collisions using $\eta\pi^\pm$ in $\gamma\gamma\pi^\pm$ events

The interest in the $\eta\pi^\pm$ final state (and also in $\eta'\pi$) is that both $J^{PC} = 1^{-+}$ hybrid candidates listed in the Particle Data Book at 1400 and 1600 MeV, respectively, were found by studying angular correlations in its final state [17]. We have the possibility of performing much improved analysis of these states.

In the $\gamma\gamma\pi^\pm$ final state, the $\gamma\gamma$ invariant mass distribution is similar as in the $\gamma\gamma\pi^+\pi^-$ final state as shown in Fig. 22 Left. Therefore, we select the η signal and show the $\eta\pi^\pm$ invariant mass in Fig. 28 (398 reconstructed events, 279 coming from the ECAL interaction trigger data sample). There is enticing structure seen, even with our limited data sample. The peaks around 1 GeV and 1.3 GeV could be due, respectively, to the $a_0(980)$ and $a_2(1320)$ resonances also observed in [20].

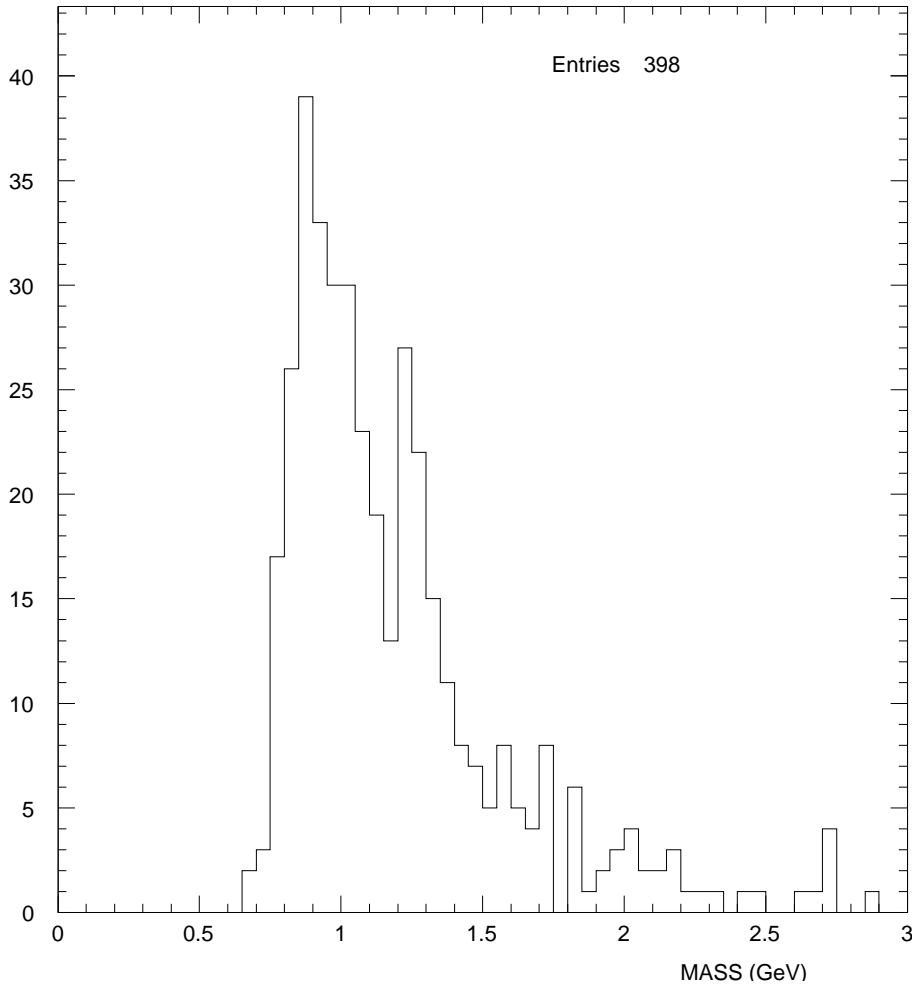


Figure 28: $\eta\pi^\pm$ mass distribution

9.7 ρ^\pm and \mathcal{R} eggeon-Exchange

The $\gamma\gamma\pi^\pm$ final state which contains the $\eta\pi^\pm$ channel, also contains the $\pi^0\pi^\pm$ channel. Fig. 29 shows the $\pi^0\pi^\pm$ invariant mass distribution (1259 reconstructed events, 894 coming from the ECAL interaction trigger data sample), which displays a very nice ρ^\pm signal with relatively low combinatoric background. This low background could be indication of the fact that the most of the ρ signal is being produced centrally and alone. Because of

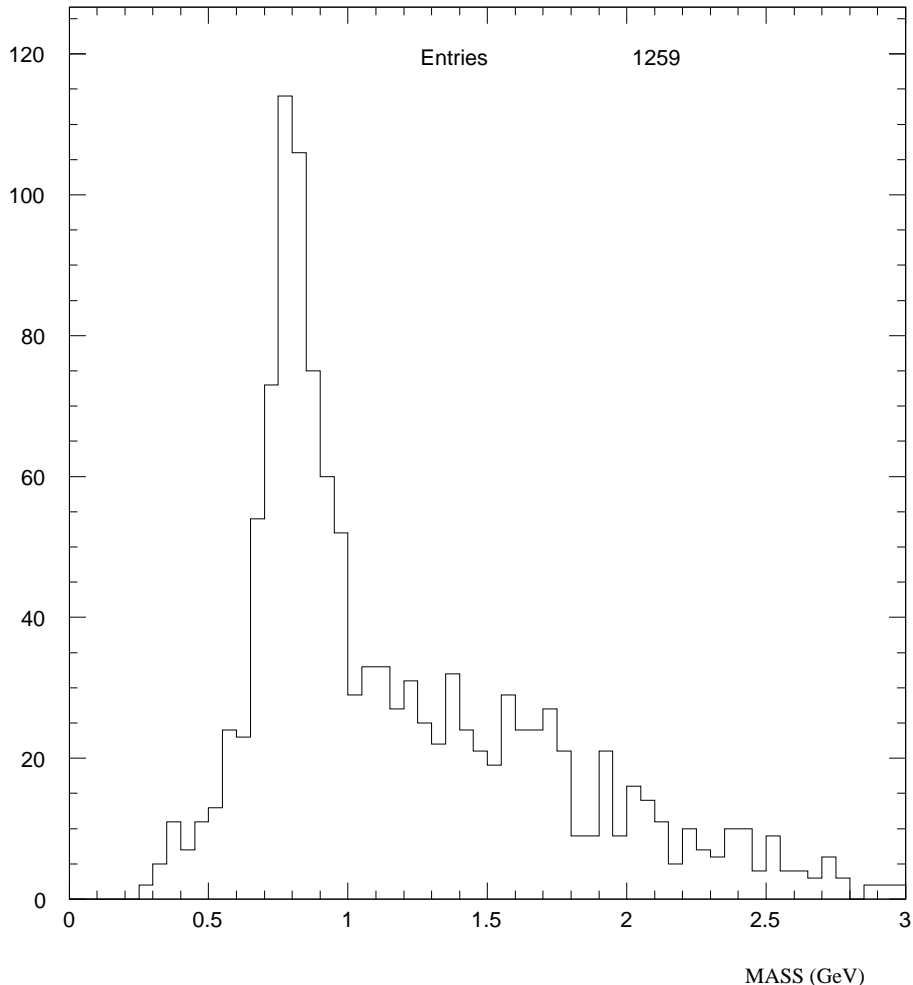


Figure 29: $\pi^0\pi^\pm$ mass spectrum in $\gamma\gamma\pi^\pm$ events.

the charge of the ρ^\pm , \mathcal{R} eggeon-Exchange must be involved. A future study of the x_F distribution of this state should be very interesting and will teach us more of \mathcal{R} eggeon-Exchange phenomenology and possible nuclear effects. We already see suggestions (not shown there) that a similar, but perhaps somewhat larger asymmetry in x_F than shown in Sect. 6.3 is present here. Thus, there may also be interesting nuclear effects in \mathcal{R} eggeon-Exchange reactions.

9.8 $\gamma\gamma$ final state

$\gamma\gamma$ events exhibit only 2 clusters in the ECAL. The upper distribution in the semilog Fig. 30 shows the invariant mass for 10,926 such events. The lower distribution shows events with $|x_F| < 0.03$. Their similarity shows that most of the events cluster around $x_F = 0$. There is a large π^0 peak (7,760 events), a much smaller η peak (500 events), but almost no events at the higher masses. This latter observation is reassuring because it implies that there are few background γ s seen. Although γ s couple to $q\bar{q}$ states in the higher mass range with very low probability, typically 10^{-5} to 10^{-6} , perhaps with the very large statistics which will be available to us, we may be able to directly observe $\gamma\gamma$ decay modes. Until now, all such information has come from $\gamma\gamma$ interactions in LEP experiments.

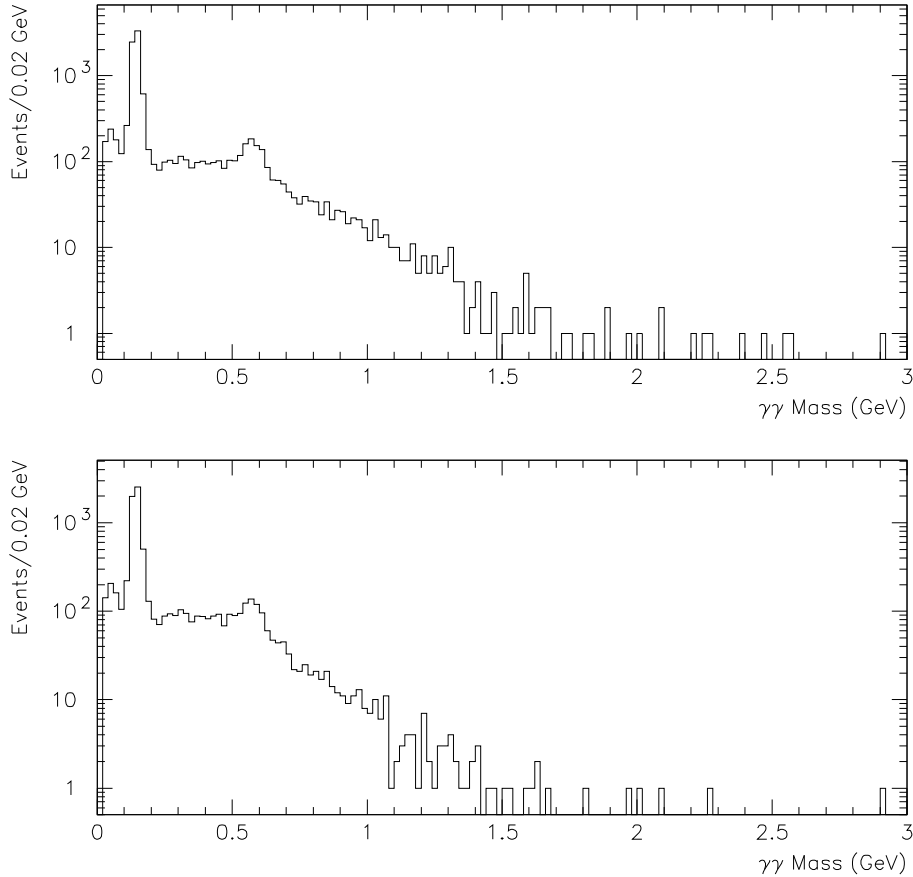


Figure 30: *Invariant mass for 10,926 $\gamma\gamma$ events. There are 7,760 events in the π^0 peak and 500 events in the η peak. The lower distribution is only for events with $|x_F| < 0.03$.*

9.9 Statistics achievable by HERA-g

We summarize here the potential of the HERA-g experiment to select centrally produced events in pN at $\sqrt{s} = 41.6 \text{ GeV}$ by developing two different scenarios of data taking:

- “SHORT TERM”: 100 hours of data taking at 1 MHz interaction rate with Carbon wire target.
- “LONGER TERM”: 10^7 seconds of data taking at 1 MHz interaction rate with Carbon wire target.

It is important to stress here that **the present proposal addresses a “SHORT TERM” scenario of the order of 100 hours duration.** The “LONGER TERM” is considered as an example to illustrate the possibilities of HERA-g in case of a longer, and still of reasonable duration, data taking period.

The running configuration is the one already explained in this proposal (see Sections 3.2, 3.3 and 7.2). For each scenario we will consider the minimum and maximum statistics achievable in all the final states studied. The minimum statistics corresponds to a live time fraction $F_{lt} = \frac{1}{5}$ and the maximum to $F_{lt} = 1$ (for the definition of F_{lt} see Sect. 7.2 and Table 6 therein). The multiplication factor M_f to be applied to the statistics available in the 2002/2003 data-taking can be calculated by using the Eqn. 8 assuming $T(\text{HERA-B}) \sim 72000 \text{ s}$, and so obtaining the extrapolation for HERA-g .

In Table 8 we show the statistics achievable by HERA-g in the two different scenarios for all the centrally produced final state considered in this proposal. The extrapolation for

Final State	100 hours of HERA-g run		10^7 s of HERA-g run	
	Min. Stat.	Max. Stat.	Min. Stat.	Max. Stat.
$\pi^0\pi^0$	$\sim 900,000$	$\sim 4,500,000$	$\sim 24,000,000$	$\sim 120,000,000$
$\pi^+\pi^-$	$\sim 1,300,000$	$\sim 6,500,000$	$\sim 36,000,000$	$\sim 180,000,000$
K^+K^-	$\sim 60,000$	$\sim 300,000$	$\sim 1,700,000$	$\sim 8,500,000$
$K_s^0K_s^0$	$\sim 5,000$	$\sim 25,000$	$\sim 140,000$	$\sim 700,000$
$\eta\pi^\pm$	$\sim 110,000$	$\sim 550,000$	$\sim 3,000,000$	$\sim 15,000,000$
$\pi^0\pi^\pm$	$\sim 360,000$	$\sim 1,800,000$	$\sim 10,000,000$	$\sim 50,000,000$
$\pi^+\pi^-\pi^0$	$\sim 360,000$	$\sim 1,800,000$	$\sim 10,000,000$	$\sim 50,000,000$
$\pi^+\pi^-\eta$	$\sim 70,000$	$\sim 350,000$	$\sim 2,000,000$	$\sim 10,000,000$
$K_s^0K^\pm\pi^\mp$	$\sim 6,000$	$\sim 30,000$	$\sim 160,000$	$\sim 800,000$
$\pi^+\pi^-\pi^+\pi^-$	$\sim 90,000$	$\sim 450,000$	$\sim 2,400,000$	$\sim 12,000,000$
$\gamma\gamma$	$\sim 4,000,000$	$\sim 20,000,000$	$\sim 110,000,000$	$\sim 550,000,000$

Table 8: .Total statistics achievable by HERA-g in two different scenarios of data taking duration (100 hours or 10^7 seconds) at 1 MHz interaction rate with Carbon wire target for all the final states presented in this proposal. For each scenario a minimal and maximal extrapolation on the achievable statistics is given.

each channel has been done using only the statistics coming from the ECAL interaction trigger run in 2002/2003.

As one can see a large variety of final states can be investigated with relevant statistics. This will allow, for example, to perform a spin-parity analysis both in the single-channel and in the coupled-channel modes. This possibility is important because it will allow on the one hand to put more constraints into the analysis, and on the other hand to measure the decay amplitudes of a given state in different channels, providing important information for identifying exotic states such as glueballs and hybrids.

The numbers reported in Table 8 show that, as already discussed in many parts of this document, even in the proposed “SHORT TERM” program, HERA- g is very competitive and can significantly improve the the existing statistics from other similar experiments in nearly every interesting centrally produced decay mode.

In a possible “LONGER TERM” program HERA- g could provide the largest available statistics in the world for this kind of analysis.

As a conclusion, in either scenario, HERA- g is a very competitive experiment given the quantity of channels that can be studied and the quality of the data, and will provide, no doubt, very important and fundamental contributions to the identification of exotic states.

10 Proposed Program

We outline here a rough chronological order of the main tasks that are needed in order to start the commissioning phase of the HERA-*g* experiment.

- Remove the ITR stations from the experimental area (3 days of access), reconfigure them (out of the experimental area) following the guidelines presented in Section 3.1 (1 month), and place them again on the experiment (7 days of access).
- Install the LAC vetoing system in the first station of the VDS system (14 days of access with opening the high vacuum parts of the VDS).
- Start the training of the detectors necessary for HERA-*g*. This phase will need the wire target insertion, and should last less than two months for the ITR. In the meantime the commissioning of Level-1 could be performed and the preparation of the run be completed.
- Data taking.

10.1 Manpower needs

The HERA-*B* experiment was well commissioned in all its parts. The DAQ and Slow Control do not need modifications to run the HERA-*g* experiment. The off-line reconstruction program must be adapted to the changed needs. Some work has been already initiated in this respect. The Monte Carlo detector geometry needs to be modified by adding the SAC (already in progress) and LAC systems.

Part of the existing HERA-*B* collaboration can help in the starting phase of a new experiment. From the hardware point of view this statement applies to all the main detectors needed by HERA-*g*: Target (Kiev), VDS (Heidelberg), RICH (Ljubljana), ECAL and Level-1 (INFN Bologna, ITEP). The OTR system, together with the gas systems and the DAQ, depend on DESY and support is expected pending the approval of this proposal. The MUON system (ITEP) is not foreseen for the planned physics program.

The most serious problem concerns the ITR group where expert knowledge is quickly disappearing. A reshuffling of the existing manpower could be nevertheless possible at least to transfer experience and knowledge for starting the ITR for HERA-*g*. The hardware interventions on ITR described in Section 3.1 should in any case be done before the end of the year 2003.

It appears clear from this survey that, if some rethinking does not happen inside the present HERA-*B* collaboration, the remaining members could nevertheless guarantee the transfer of knowledge and participate in the start of operation of the needed detectors. The potential of HERA-*g* to provide significant new results rapidly was recognized by the community of experts present at the Hadron 2003 conference [21], with some groups expressing interest in joining the project.

11 Conclusions

We have demonstrated that the HERA-*B* spectrometer is well-suited to study central systems produced in collisions of *P*omeron and *R*eggeons. The search for *O*dderon-Exchange in the central production of states with $I=0$ and $C=-1$ can also be carried out. There appears to be no near-term competition to the HERA-*g* capabilities.

The only necessary modification to the existing HERA-*B* spectrometer is to replace the four silicon detectors in the first measuring station of the VDS by four scintillation counters to be used as part of the rapidity-gap veto system in our Level-1 trigger. The ITEP group reports that this can be very rapidly done, within one month of receiving DESY approval for the first HERA-*g* run.

Double-*P*omeron -Exchange phenomenology is shown to be in agreement with predictions from Experiment UA8 run at the SPS-Collider with 630 GeV c.m. energy. This suggests that *R*eggeon -Exchange and *O*dderon -Exchange processes should also be identifiable.

The results of the preliminary analysis with our small data sample allow us to conclude that :

- The experimental resolutions are adequate both for charged and neutral final states. The background levels are sufficiently low that high quality spectroscopic data can be taken with masses up to 4 GeV for final states with both neutral and charged particles as well as strange mesons.
- The rate estimates we give are solid since they are derived by the analysis of the acquired data sample. With a run duration of order 100 hours, we will be able to acquire more than 1000 times the data samples presented in this proposal. As detailed in Sect. 9.9, this sample would be comparable to and, in some cases, many times larger than any existing centrally produced sample.
- The huge data sample will allow considerable progress in the understanding of glueballs and states with exotic quantum numbers. Additionally, valuable insights into *P*omeron, *R*eggeon, *O*dderon processes can also be expected.

Thus we believe we can produce a splendid physics program using the HERA-*B* detector in the manner proposed here.

References

- [1] D. Barberis et al., Phys. Lett. B 453 (1999) 325.
- [2] C. McNeile and C. Michael, Phys. Rev. D 63 (2001) 114503;
D. Weingarten, Nucl. Phys. Proc. Suppl. 53 (1997) 232; *ibid* 63 (1998) 194; *ibid* 73 (1999) 249;
C.J. Morningstar and M. Peardon, Phys. Rev. D 56 (1997) 4043;
G. Bali et al. (SESAM Collaboration) Nucl. Phys. Proc. Suppl. 63 (1997) 209;
F.E. Close and M.J. Teper, Report No. RAL-96-040/OUTP-96-35P;
J. Sexton et al. (IBM Collaboration), Phys. Rev. Lett. 75 (1995) 4563.
- [3] C. Morningstar, Nucl. Phys. Proc. Suppl. 90 (2000) 214;
C. McNeile, hep-lat/9904013;
P. Lacock and K. Shilling, Nucl. Phys. Proc. Suppl. 73 (1999) 261;
C. Bernard et al., Phys. Rev. 56 (1997) 7039;
P. Lacock, C. Michael, P. Boyle and P. Rowland, Phys. Lett. 401 (1997) 308.
- [4] K. Hagiwara et al. (Review of Particle Physics), Phys. Rev. D 66 (2002) 010001.
- [5] G. Avoni et al., Nucl. Instr. and Meth. A461 (2001) 332.
- [6] HERA-*B* Technical Design Report, DESY-PRC 95/01, January 1995.
- [7] A. Brandt et al., [UA8 Collaboration], Phys. Letters B 297 (1992) 417.
- [8] C. Adloff et al. [H1 Collaboration], Z. Phys. C 76 (1997) 613.
- [9] D. Robson, Nucl. Phys. B 130 (1977) 328; Yu.A. Simonov, Phys. Lett. B 249 (1990) 514.
- [10] A. Brandt et al. [UA8 Collaboration], Eur. Phys. Jour. C 25 (2002) 361.
- [11] D. Barberis et al. [WA-102 Collaboration], Phys. Lett. B 474 (2000) 423; Phys. Lett. B 397 (1997) 339.
- [12] F.E. Close and A. Kirk, Phys. Lett. B 397 (1997) 333;
F.E. Close and G.A. Schuler, Phys. Lett. B 464 (1999) 279;
F.E. Close and G.A. Schuler, Phys. Lett. B 458 (1999) 127.
- [13] A. Kirk, “Resonance production in central pp collisions at the CERN Omega Spectrometer”, hep-ph/0008053.
- [14] D. Barberis et al., Phys. Lett. B 453 (1999) 316.
- [15] D. Barberis et al., Phys. Lett. B 453 (1999) 305.
- [16] Obelix Collaboration, Phys. Lett. B 462 (1999) 453.
- [17] See references for hybrid candidates in “NON- $q\bar{q}$ CANDIDATES in The Review of Particle Physics [4].
- [18] D. Barberis et al., Phys. Lett. B 413 (1997) 217.
- [19] Peter E. Schlein, Phys. Lett. B 332 (1994) 136.
- [20] D. Barberis et al., Phys. Lett. B 488 (2000) 225.

[21] P. Schlein, “ HERA- g , a new experiment for glueball and hybrid studies at DESY with the HERA- B detector”, presented at the X International Conference on Hadron spectroscopy (Hadron 2003) - Aschaffenburg, September 4th 2003